

RPI-TR-PT-6808



# ***PROJECT TUBEFLIGHT***

DUANE E. CROMACK

ANALYSIS OF THE EFFECTS OF WALL PERFORATIONS  
ON THE PERFORMANCE OF A VEHICLE IN A TUBE

TR PT 6808

ANALYSIS OF THE EFFECTS OF WALL PERFORATIONS  
ON THE PERFORMANCE OF A VEHICLE IN A TUBE

by

Duane E. Cromack

This research was supported in part by a National Science Foundation Grant and in part by the United States Department of Transportation under Contract No. C-117-66 (Neg.)

This report is taken from part of a thesis submitted in partial fulfillment of the requirements for the degree of Doctor of Engineering in the Division of Fluid, Chemical and Thermal Processes at Rensselaer Polytechnic Institute

DIVISION OF FLUID, CHEMICAL AND THERMAL PROCESSES  
RENSSELAER POLYTECHNIC INSTITUTE  
TROY, NEW YORK

December 1968

### ACKNOWLEDGMENT

The author wishes to express his appreciation to Dr. Joseph V. Foa for his helpful suggestions and guidance throughout the course of this work and to Dr. Theodore R. Goodman for several stimulating discussions.

## TABLE OF CONTENTS

|  | Page |
|--|------|
| ACKNOWLEDGMENT                                       | ii   |
| TABLE OF CONTENTS                                    | iii  |
| LIST OF FIGURES                                      | v    |
| ABSTRACT   | vii  |
| NOMENCLATURE   | viii |
| 1. INTRODUCTION                                      | 1    |
| 2. THEORETICAL ANALYSIS                              | 5    |
| 2.1. Equations of Motion                             | 5    |
| 2.1.1. Boundary Conditions                           | 6    |
| 2.2. The Vehicle as a Drag Disc                      | 7    |
| 2.2.1. Inviscid Flow                                 | 7    |
| 2.2.2. Viscous Flow                                  | 12   |
| 2.3. The Thrust Generator as an Actuator Disc        | 15   |
| 2.3.1. Inviscid Flow                                 | 15   |
| 2.3.2. Viscous Flow                                  | 18   |
| 2.4. The Vehicle as Matched Drag and Actuator Discs  | 20   |
| 2.4.1. Drag - Actuator Disc Combination              | 20   |
| 2.4.2. Actuator - Drag Disc Combination              | 24   |
| 2.4.3. Doublet                                       | 28   |
| 3. EXPERIMENTAL APPARATUS AND PROCEDURE              | 31   |
| 3.1. Aerodynamic Characteristics of Perforated Tubes | 31   |
| 3.1.1. Experimental Facility                         | 31   |
| 3.1.2. Test Procedure                                | 32   |
| 3.1.3. Data Reduction                                | 33   |

|   | Page |
|---|------|
| 3.2. Drag Disc in a Perforated-Wall Tube            | 34   |
| 3.2.1. Experimental Facility                        | 34   |
| 3.2.2. Test Procedure                               | 34   |
| 3.2.3. Data Reduction                               | 35   |
| 4. DISCUSSION OF RESULTS                            | 36   |
| 4.1. The Vehicle as a Drag Disc                     | 37   |
| 4.2. The Thrust Generator as an Actuator Disc       | 42   |
| 4.3. The Vehicle as Matched Drag and Actuator Discs | 43   |
| 5. CONCLUSIONS                                      | 47   |
| 6. REFERENCES                                       | 49   |
| FIGURES   | 51   |
| APPENDIX  | 81   |

LIST OF FIGURES

| Figure Number | Title   | Page |
|---------------|---|------|
| 1             | Wall-Fixed and Disc Fixed Frames of Reference   | 51   |
| 2             | Typical Pressure and Velocity Distributions   | 52   |
| 3             | Simulated Internally Propelled Vehicle<br>Pressure and Velocity Distributions   | 53   |
| 4             | Schematic - Perforated-Wall Test Facility   | 54   |
| 5             | Schematic - Perforated Tube - Drag Disc Facility  | 55   |
| 6             | Photographs Showing Perforated Tube - Drag Disc Facility  | 56   |
| 7             | Relation Between Cross Flow Velocity and the<br>Pressure Difference Across the Wall   | 57   |
| 8             | Velocity $U_d$ Through the Disc as a Function of the<br>Disc Porosity   | 58   |
| 9             | Pressure Difference Across the Wall at the Drag Disc<br>Versus Disc Porosity  | 59   |
| 10            | Disc Drag Coefficient as a Function of Disc Porosity<br>for Various Wall Porosities   | 60   |
| 11            | Disc Drag Coefficient as a Function of Disc Porosity<br>for Various Tube Wall Friction Factors  | 61   |
| 12            | Drag Disc Alone - Inviscid Flow Pressure and Velocity<br>as Functions of Distance from the Drag Disc for Various<br>Wall Porosities           | 62   |
| 13            | Drag Disc Alone - Viscous Flow<br>Pressure and Velocity as Functions of Distance<br>from the Drag Disc for Various Wall Porosities            | 63   |
| 14            | Drag Disc Alone - Viscous Flow<br>Pressure and Velocity as Functions of Distance<br>from the Drag Disc for Various Tube Wall Friction Factors | 64   |
| 15            | Drag Disc Alone - Stationary Tube<br>Wall Pressure and Velocity as Functions<br>of Distance from the Drag Disc                                | 65   |
| 16a           | Drag Disc Alone - Stationary Wall<br>Velocity as a Function of Distance<br>from the Drag Disc   | 66   |

| Figure<br>Number | Title   | Page |
|------------------|---|------|
| 16b              | Drag Disc Alone - Stationary Wall<br>Pressure as a Function of Distance<br>from the Drag Disc                               | 67   |
| 17               | Static Pressure Traverse Immediately Behind Drag Disc   | 68   |
| 18               | Velocity Profiles in the Neighborhood of a Drag Disc<br>in a Perforated Wall Tube   | 69   |
| 19               | Perforated Disc Showing Direction of Velocity<br>and Pressure Traverse  | 70   |
| 20               | Ratio of Viscous to Inviscid Flow Drag Coefficients<br>as a Function of Wall Porosity for Various Disc<br>Porosities        | 71   |
| 21               | Effect of Tube Wall Porosity on the Effective Drag<br>Ratio at Vehicle Terminal Speeds                                      | 72   |
| 22               | Actuator Disc Alone<br>Pressure and Velocity as Functions of Distance<br>from the Actuator Disc for Various Wall Porosities | 73   |
| 23               | Simulated Internally Propelled Vehicle<br>Effect of Variation of Wall Porosity on Pressure<br>and Velocity Distributions    | 74   |
| 24               | Simulated Internally Propelled Vehicle<br>Effect of Viscosity on Pressure and Velocity<br>Distributions                     | 75   |
| 25               | Simulated Internally Propelled Vehicle<br>Effect of Vehicle Length on Pressure and Velocity<br>Distributions                | 76   |
| 26               | Simulated Internally Propelled Tubeflight Vehicle<br>in a 5 Per Cent Porous Tube  | 77   |
| 27               | Simulated Internally Propelled Vehicles<br>Effect of Fore or Aft Positioning of Thrust Generator                            | 78   |
| 28               | Simulated Internally Propelled Vehicle<br>Drag Coefficient as a Function of Disc Porosity<br>for Various Wall Porosities    | 79   |
| 29               | Simulated Internally Propelled Vehicle<br>Drag Coefficient as a Function of Wall Porosity                                   | 80   |

## ABSTRACT

The flow induced by a vehicle traveling through a porous-wall tube is analyzed as a one-dimensional incompressible flow steady in the vehicle-fixed frame of reference. The pressure and velocity fields are determined for both non-viscous and viscous flows, for varying vehicle blockage ratios, for externally and internally propelled vehicles, and for various tube-wall porosities.

The externally propelled vehicle is represented by a porous drag disc and the results of the investigation show that with this type of propulsion even small wall porosities - of less than 10 per cent - can be very effective in reducing the extent of the disturbed flow field and the drag of the vehicle. The internally propelled vehicle is represented by combinations of a drag disc and an actuator disc, at appropriate distances from one another and coupled to produce equal and opposite forces, i.e., a thrust equal to the drag. The drag of the internally propelled vehicle also decreases with increasing wall porosity, up to a critical value which depends on the vehicle blockage and length. This critical wall porosity is 10 per cent for a vehicle blockage of 40 per cent and a vehicle length of 5 times the tube radius.

## NOMENCLATURE

|             |  |
|-------------|--|
| $A_h$       | hole area per unit length of tube  |
| $C_c$       | contraction coefficient  |
| $C_D$       | non-dimensional drag coefficient   |
| $C_f$       | flow coefficient for the flow through the wall   |
| $d$         | hole diameter  |
| $D$         | tube diameter  |
| $\dot{m}_w$ | elemental mass flow rate through the tube wall   |
| $f$         | friction force per unit mass of fluid  |
| $n$         | number of holes per unit length of tube  |
| $p$         | static pressure in the tube  |
| $P$         | $= p/\frac{1}{2} \rho u_w^2$ , normalized pressure in the tube                         |
| $p_a$       | ambient static pressure  |
| $\dot{Q}$   | volume flow rate   |
| $q$         | dynamic pressure   |
| $r$         | tube radius  |
| $u$         | local flow velocity relative to the disc   |
| $U$         | $= u/u_w$ , normalized local velocity  |
| $u_s$       | x-directed velocity of the mass entering or leaving through the tube wall              |
| $u_w$       | velocity of the wall relative to the disc  |
| $V_w$       | average flow velocity through each hole in the wall                                    |
| $\alpha$    | tube cross-sectional area  |
| $\beta$     | disc porosity (ratio of the open area to the total area times contraction coefficient) |
| $\psi$      | $= nd^2/4D$ , wall porosity  |
| $\rho$      | mass density   |

## 1. INTRODUCTION

This report deals with the effects of wall perforations on the propulsion of a vehicle traveling through a tube. These effects are evaluated for different vehicle blockage ratios, for external and internal modes of propulsion, and for both viscous and non-viscous flows through one-dimensional incompressible flow analyses. Two experiments, aimed at the verification of an assumed relation for the flow through the wall and of a portion of the analysis relating to externally propelled vehicles, are also reported.

### Historical Review

The existing literature on the subject of this investigation falls into two general areas - flow through perforated walls and propulsion of vehicle in tubes. Several investigators<sup>1-6</sup> have considered the problem of fluid flows in ducts with porous walls. In general, the theoretical studies have been limited to laminar incompressible flow for a finite-length system and have yielded solutions to the Navier-Stokes equations based on the key assumption of a uniform flow velocity through the wall. This assumption can be valid only for a finite-length porous section of small porosities with a constant pressure difference across the wall. This is not a reasonable assumption for an infinitely long porous tube which is the case in the present investigation. For the model of this report, the pressure in the tube, hence the driving potential for inflow or outflow through the tube wall, is dependent upon the vehicle mode of propulsion and on the distance from the vehicle.

Goodman<sup>7,16</sup> avoided the restrictive assumption of a constant velocity through the wall and proposed the perforated wall boundary

condition derived in terms of a potential flow. This boundary condition is based on the linerized Bernoulli equation giving the pressure difference across the wall proportional to the time rate of change of the velocity potential, and is undoubtedly correct for the near field problem that Goodman was considering. On the other hand, as pointed out by Foa, non-steady effects in the flow through the wall are unimportant wherever the time required for the pressure to change appreciably inside the tube is very long compared to the travel time of pressure waves over a distance equal to the thickness of the wall -- a condition which is surely satisfied everywhere in the far-field.\* Therefore, the flow through the wall can accordingly be taken to be everywhere and at each instant proportional to the square root of the local and instantaneous pressure difference across the wall.

Numerous aspects of problems associated with the propulsion of vehicles traveling through tubes have been reported with an excellent summary of these results presented recently by Foa<sup>8</sup>. Of particular significance to the present investigation are the results of Cromack and Iyer<sup>9</sup> who experimentally evaluated the effects of wall porosity on both externally and internally propelled vehicles. For the low test speeds and a single blockage ratio, it was found that a wall porosity of only 10 per cent was needed to reduce the effective drag of the vehicle in a tube to that of a vehicle on an open track.

This investigation deals with the effects of both blockage ratio and mode of vehicle propulsion (external or internal). The externally

---

\* The fact that local rates of change of conditions are significant only in the near field -- and, even there, only where the slope of the meridional contour of the vehicle is large -- has been recognized by Goodman in a private communication.

propelled or wheel driven vehicle generates a flow in the direction of the motion of the vehicle because of the region of increased pressure ahead of the vehicle. A drop in pressure occurs across the vehicle. Part of the object of this investigation is to determine what occurs behind the vehicle. The internally propelled or propeller driven vehicle derives its thrust by the fore-to-aft transfer of air around the vehicle. Thus a region of reduced pressure exists ahead of the propeller with an increase in pressure across the propeller. In the vehicle-fixed frame of reference, the flow is steady and would appear as shown in Fig. 2. Because of the different flow fields generated by the two modes of propulsion, the effect of wall porosity is expected to be significantly different.

#### Statement of the Problem

The purpose of this investigation is to determine analytically the effect wall perforations have on the performance of externally and internally propelled vehicles of various blockage ratios. The model considered is an infinitely long, uniformly porous tube with the flow induced by the vehicle assumed to be incompressible, one-dimensional and steady in the vehicle frame of reference. Because of the similarity of the induced flow fields, the externally propelled vehicle is represented by a porous disc or drag disc placed normal to the tube axis. The porosity of the disc is specified by the vehicle blockage ratio.

An ideal propeller or actuator disc generates a low pressure region ahead and a rise in pressure across itself. With this configuration, the flow is accelerated towards the propeller at a velocity greater than the wall velocity. The actuator disc alone represents a thrust generator.

The internally propelled vehicle, on the other hand, can be represented by a suitably matched combination of drag and actuator discs.

For steady level motion, the drag disc solution must be matched to the actuator disc solution with the correct amount of inflow between the two discs, such that the thrust equals the drag.

The following assumptions are made:

1. The flow is treated as incompressible, one-dimensional, and steady in the disc-fixed frame of reference.

2. The flow through the wall is proportional to the square root of the pressure difference across the wall. This assumption implies that each tube-wall perforation acts as an orifice, with no mutual interference, and that the flow through the wall is quasi-steady.

Both viscous and non-viscous flows are considered. Non-viscous flow means that there is no force on the flow due to the moving wall.

Although this analysis is limited to moderate speeds due to the assumption of incompressibility, the model is capable of revealing the effects of the porous tube for the different modes of propulsion and for different blockage ratios. Initially, the drag and actuator discs will be analyzed individually. They will then be combined to represent the internally propelled vehicle.

## 2. THEORETICAL ANALYSIS

### 2.1 Equations of Motion

The one-dimensional steady-flow momentum and continuity equations for the flow of an incompressible viscous fluid through a tube with perforated walls, as derived in the Appendix, are

$$dP = -2(2U - U_s) dU + 2C_f(1-U)/|1-U| dX \quad 2.1$$

$$dU = \frac{2\psi V_w(x)}{u_w} dX \quad 2.2$$

where  $U_s = u_s/u_w$  is the axial velocity of the flow that crosses the control volume boundary. Thus  $U_s = U$  for outflow and  $U_s = 1$  for inflow.  $V_w(x)$  is the average velocity through a given hole and is directly proportional to the pressure difference across the tube wall.  $V_w(x)$  may be positive (inflow) or negative (outflow), and is given in the Appendix as

$$V_w(x)/u_w = -C_f \sqrt{P - P_a} \quad (\text{Outflow}) \quad 2.3a$$

$$V_w(x)/u_w = C_f \sqrt{P_a - P} \quad (\text{Inflow}) \quad 2.3b$$

In these expressions for the flow through the wall, each hole is assumed to be an orifice with a flow coefficient  $C_f$ .

For inviscid flow ( $C_f = 0$ ), eq. 2.1 can be integrated directly and combined with equations 2.2 and 2.3. After the appropriate

boundary conditions are established the resulting integrated equations define the entire inviscid flow field.

In the case of viscous flow, the solution of eqs. 2.1 and 2.2 is more difficult. A numerical solution of the two equations simultaneously is possible once the initial conditions are established. Solutions for the regions ahead of and behind the vehicle must be found separately and matched at the vehicle. Thus the overall solution requires solving a two-point boundary value problem numerically as two initial value problems. The initial conditions, however, must be determined in terms of the solutions to the flow equations for the up-stream and down-stream regions. Solutions require assuming the conditions at the vehicle (initial conditions), integrating with respect to distance, then adjusting the initial conditions until the up-stream and down-stream boundary conditions are satisfied.

2.1.1. Boundary Conditions. A pressure difference across the porous wall cannot be sustained, hence, at some distance ahead of and behind the vehicle, the pressure in the tube must be atmospheric, i.e.  $P - P_a = 0$ . Furthermore, the effect of viscosity is to bring the flow to rest relative to the tube wall. In the vehicle or disc-fixed frame of reference then, the viscous-flow boundary condition for the velocity at some distance from the vehicle, is  $u = u_w$  or  $U = 1$ . For the stationary wall case, the velocity must approach zero.

For inviscid flow, changes in velocity cease when the pressure in the tube becomes atmospheric but the flow may not be at rest relative to the wall. At some distance ahead of the vehicle, the flow is undisturbed, thus the up-stream boundary conditions are  $P - P_a = 0$  and  $U = 1$ .

In the wake of the vehicle, however, the magnitude of the inviscid flow velocity depends on the mode of propulsion and must be determined from the detailed analysis of each particular case.

## 2.2. The Vehicle as a Drag Disc

### 2.2.1. Inviscid Flow

2.2.1.1. X < 0 -- OUTFLOW. Ahead of the disc outflow occurs due to the increased pressure in the tube. Equation 2.1 with  $C_r = 0$  and  $U_s = U$  yields upon integration

$$P - P_a = 1 - U^2 \quad 2.4$$

where the constant of integration has been evaluated at some distance ahead of the disc where  $P = P_a$  and the flow is at rest relative to the tube wall (i.e.  $U = 1$ ). Substitution of eqs. 2.4 and 2.3a into 2.2 gives

$$dU = -2\psi C_f \sqrt{1 - U^2} dX$$

and upon integration

$$U = \sin(-\lambda X + C_1) \quad 2.5$$

where

$$\lambda = 2\psi C_f$$

and

$$C_1 = \sin^{-1} U_d .$$

Equation 2.5 for  $U = 1$  yields

$$X_o = \frac{\pi/2 - C_1}{-\lambda} \quad 2.6$$

Equations 2.4 and 2.5 describe the inviscid flow pressure and velocity distribution ahead of the drag disc as functions of the wall porosity. The length of disturbed flow ahead of the disc is given by eq. 2.6 and is shown to be inversely proportional to the wall porosity.

2.2.1.2.  $X > 0$  -- INFLOW. The pressure increases to a value greater than atmospheric ahead of the disc and is expected to drop to a value below atmospheric behind the disc. The flow is assumed to be incompressible with no inflow or outflow through the tube wall in the immediate vicinity of the disc. Therefore, the flow must accelerate through the disc due to the area constriction and then expand back to fill the tube a short distance behind the disc. Figure 2 depicts the flow model and shows typical pressures and velocities in the disc frame of reference. Station 2' is defined as the location behind the disc where the flow again fills the tube cross section after accelerating through the disc. At 2' the pressure is  $P_2$ , and the velocity is  $U_d$ . No assumption is made as to the magnitude of  $P_2$ , relative to  $P_a$ . At station 2, immediately behind the disc, the pressure is  $P_2$  and the velocity is  $U_d/\beta$ , where  $\beta$  is defined as the ratio of the open area to the total area of the disc times a contraction coefficient.

The one-dimensional flow eqs. 2.1 and 2.2 must be satisfied from 2' to station 3 where  $P - P_a = 0$  and no further changes occur. Since the flow is assumed to be non-viscous, the only mechanism to cause the

flow to change is a pressure difference across the wall. At station 3,  $P = P_a$  since the pressure must return to atmospheric due to the porous walls but the magnitude of the velocity is not known and must be determined from the analysis.

If  $P_a > P_2$ , inflow occurs and eq. 2.1, for inflow and  $C_r = 0$ , becomes

$$dP = -2(2U-1)dU \quad 2.7$$

Inflow means an increase in velocity or positive  $dU$ . Furthermore,  $dP$  must be positive for the pressure to return to atmospheric, making  $dP/dU$  positive. Equation 2.7 then shows that inflow cannot occur behind the drag disc for inviscid flow unless  $U < .5$ . For  $U > .5$ ,  $dP/dU$  cannot be positive so no inflow can occur.

$U_d < .5$ . Equation A-8, obtained by eliminating  $P$  between eqs. 2.2, 2.3b and 2.7 gives

$$\frac{d^2U}{dX^2} = \lambda^2(2U-1) \quad 2.8$$

Integration of eq. 2.8 yields, for  $U = U_d$  at  $X = 0$ ,

$$U = .5 + (U_d - .5) e^{-\sqrt{2}\lambda X} \quad 2.9$$

Equations 2.9 and A-3 show that  $P = P_a$  when  $U = .5$ . Thus for  $U_d < .5$ , inflow occurs behind the drag disc and  $U$  approaches  $.5$  exponentially.

It should be noted that if  $P_a < P_{2'}$ , outflow occurs and eq. 2.1 becomes

$$dP = -2U dU \quad 2.10$$

Outflow results in a negative  $dU$  and eq. 2.10 then gives a positive  $dP$ . For  $P_a < P_{2'}$ , however, a negative  $dP$  is required for the pressure to return to atmospheric.

Thus the only conditions satisfying eqs. 2.1 and 2.2 are: for  $U_d \geq .5$ ,  $P_{2'} = P_a$  and consequently no inflow or outflow occurs, leaving  $U = U_d$  everywhere downstream of  $2'$ ; and for  $U_d < .5$ ,  $U_3 = .5$ , and  $P_a - P_{2'}$  is given by

$$P_a - P_{2'} = 2(U_d^2 - U_d + .25) \quad 2.11$$

and the velocity distribution by eq. 2.9.

2.2.1.3. X = 0. Constant total energy flow is assumed through the disc, thus the Bernoulli eq. from 1 to 2 gives

$$P_1 + \frac{1}{2} \rho U_d^2 = P_2 + \frac{1}{2} \rho \left( \frac{U_d}{\beta} \right)^2$$

or in normalized form

$$P_1 - P_2 = U_d^2 \left( \frac{1}{\beta^2} - 1 \right) \quad 2.12$$

$U_d \geq .5$ . The momentum equation written between 2 and 2' is,  
for  $U_d \geq .5$  and  $P_{2'} = P_a$

$$P_2 \alpha + \rho \alpha U_d \left( \frac{U_d}{\beta} \right) = P_{2'} \alpha + \rho \alpha U_d^2$$

since the velocity at 2 is  $u_d/\beta$  because of the area constriction. The assumption has been made that no inflow or outflow occurs between 1 and 2' thus  $u_{2'} = u_d$ . Normalized, this equation becomes, for  $P_{2'} = P_a$ ,

$$P_a - P_2 = 2 U_d^2 \left( \frac{1}{\beta} - 1 \right) \quad 2.13$$

Equations 2.4, 2.12 and 2.13 combined describe the entire inviscid flow field influenced by the drag disc. Combining these equations and solving for  $U_d$  as a function of  $\beta$  yields

$$U_d = \frac{\beta}{\sqrt{2\beta^2 - 2\beta + 1}} \quad 2.14$$

Now the above equations can be solved completely for a given value of  $\beta$ , that is, for any given disc porosity.

$U_d < .5$ . For  $U_d < .5$ ,  $P_{2'} < P_a$  and inflow occurs.

Equation 2.13 then becomes

$$P_{2'} - P_2 = 2 U_d^2 \left( \frac{1}{\beta} - 1 \right) \quad 2.15$$

Equations 2.4, 2.11, 2.12 and 2.15 combined can be solved for  $U_d$  in terms of  $\beta$  to get

$$U_d = \frac{\beta}{(1-2\beta)} \left[ -\beta \pm \sqrt{\beta^2 - 3\beta + 1.5} \right] \quad 2.16$$

The drag of the disc is obtained from a momentum balance across the disc, i.e. between 1 and 2' which gives the drag  $D$ , as

$$D = (P_1 - P_2') \alpha$$

The drag coefficient defined by

$$C_D \equiv \frac{D}{\frac{1}{2} \rho U_w^2 \alpha}$$

becomes

$$C_D = P_1 - P_2'$$

or from eqs. 2.12 and 2.13

$$C_D = U_d^2 \left( \frac{1-\beta}{\beta} \right)^2 \quad 2.17$$

#### 2.2.2. Viscous Flow

For viscous flow, eq. 2.1 must be integrated numerically because of its non-linear nature. Equations 2.1 and 2.2 can be solved simultaneously using a Runge-Kutta forward integration scheme providing initial conditions at the disc for the pressure and velocity are known. This means that  $P_1 - P_a$  and  $U_d$  must be known for a given wall porosity and friction factor. However, the velocity through the disc is not known for

a given disc porosity  $\beta$ , until the pressure difference ( $P_1 - P_2$ ) across the disc is determined. For viscous flow, this pressure difference depends on the integrated frictional forces ahead of and behind the disc.

Thus the problem of solving the momentum and continuity equations for viscous flow is an iterative one of solving a two-point boundary-value problem with matching conditions at the disc. A closed form approximate solution can be obtained for the viscous problem by substituting the inviscid velocity distribution into eq. 2.1 and integrating.

2.2.2.1.  $X < 0$  -- OUTFLOW. For  $X < 0$  the velocity  $U$ , was given by eq. 2.5 as

$$U = \sin(-\lambda X + C_1) \quad 2.5$$

Then

$$dU = -\lambda \cos(-\lambda X + C_1) dX$$

Substitution into eq. 2.1 for outflow with  $U_s = U$  and integration yields

$$P_1 - P_2 = 1 - U_d^2 + \frac{2C_T}{\lambda} \left\{ \frac{3}{2} \left( \frac{\pi}{2} - C_1 \right) - 2 \cos C_1 + \frac{\sin 2C_1}{4} \right\} \quad 2.18$$

The validity or degree of approximation of eq. 2.18 can be determined by assuming a value of  $U_d$  and for specified wall porosity and friction factor, calculating  $P_1 - P_2$ . This pressure and the assumed  $U_d$  then become the initial values for the numerical integration of eqs. 2.1 and 2.2. Generally no more than two iterations are needed to find the correct value of pressure  $P_1 - P_2$  for a given  $U_d$  such

that, upon numerical integration, the boundary condition of  $P - P_a = 0$  and  $U = 1$  can be satisfied.

2.2.2.2.  $X > 0$  -- INFLOW. Recall that for inviscid flow, the conditions behind the disc were found to be  $P_2 = P_a$  and  $U = U_d$  for  $U_d \geq .5$ , and for  $U_d < .5$ , inflow occurs and  $P_2 < P_a$ . The amount of wall porosity had no effect on the magnitude of the pressures at the disc for inviscid flow. For viscous flow, however, the effect of the wall is felt and the frictional force of the wall on the flow will bring the flow to rest relative to the wall. This means that the downstream boundary conditions are  $P_3 = P_a$  and  $U_3 = 1$ , thus requiring inflow behind the disc in order to satisfy continuity.

Equation A-6 of the Appendix,

$$\frac{dP}{dU} = -2(2U-1) + \frac{2C_r(1-U)/|1-U|}{\lambda \sqrt{P_a - P}} \quad \text{A-6}$$

obtained by eliminating  $dX$  between eqs. 2.1 and 2.2 shows  $dP/dU$  may be positive, negative, or zero depending on whether the friction term is greater than, less than or equal to the momentum term. For all values of  $U < .5$ ,  $dP/dU$  is positive. Furthermore,  $dP/dU$  is zero when

$$\sqrt{P_a - P} = \frac{C_r(1-U)/|1-U|}{\lambda(2U-1)}$$

Thus,  $dP/dU$  may be zero for any value of  $U$  and  $P_a - P$  depending on the magnitude of  $C_r/\lambda$ , a parameter relating the friction coefficient and the wall porosity. The particular solution of eq. A-6, or eqs. 2.1 and 2.2 simultaneously, which satisfy the conditions behind the drag disc, however, is  $P_a - P = 0$  when  $U = 1$ .

Numerical solutions to eqs. 2.1 and 2.2 for inflow behind the drag disc can be obtained by assuming a value of  $P_2' - P_a$  for a given  $U_d$  and iterating on  $P_2' - P_a$  until the downstream boundary conditions of  $P_a - P = 0$  and  $U = 1$  are simultaneously satisfied.

2.2.2.3.  $X = 0$ . Once the values of  $P_1 - P_a$  and  $P_a - P_2'$  have been obtained for any prescribed values of friction factor, wall porosity and  $U_d$ , then the corresponding value of disc porosity can be found from eqs. 2.12 and 2.15 which gives

$$\beta = \left( \frac{1}{\phi - 1} \right) \left[ -1 \pm \sqrt{\phi} \right] \quad 2.20$$

where

$$\phi = \frac{P_1 - P_a + P_a - P_2'}{U_d^2}$$

### 2.3. The Thrust Generator as an Actuator Disc

Consider next an actuator disc or propeller operating in a porous tube. In the disc-fixed frame of reference, a reduction in pressure occurs ahead of the disc causing inflow, thus an increase in the flow velocity. Energy is added at the disc resulting in a pressure jump across the disc. The actuator disc alone might be viewed as a propeller driven vehicle which has no aerodynamic drag but experiences rolling resistance equal to the thrust of the propeller.

#### 2.3.1. Inviscid Flow

2.3.1.1.  $X \leq 0$  -- INFLOW. Ahead of the actuator disc, inflow occurs due to the reduced pressure in the tube. Equation 2.1 with  $C_T = 0$  yields, upon integration

$$P_a - P = 2(U^2 - U)$$

2.21

where the constant of integration has been evaluated at some distance ahead of the disc where  $P_a = P$  and the velocity is at rest relative to the tube wall (i.e.  $U = 1$ ). Substitution of eqs. 2.21 and 2.3b into 2.2 and integration yields

$$U = \frac{1}{2} \left[ 1 + \cosh(\lambda'X + C_2) \right]$$

2.22

where

$$C_2 = \cosh^{-1}(2U_d - 1)$$

and

$$\lambda' = 2\sqrt{2} \psi C_f$$

Equation 2.22, for  $U = 1$  gives

$$X_0 = -C_2 / \lambda'$$

2.23

Equations 2.21 and 2.22 describe the pressure and velocity distribution ahead of the actuator disc as a function of the wall porosity for inviscid flow. The distance of disturbed flow ahead of the disc is given by eq. 2.23 and is shown to be inversely proportional to the wall porosity and the flow coefficient.

Immediately ahead of the disc (at  $X = 0$ ) the pressure is  $P_1$  and the velocity is  $U_d$ . Equation 2.21, evaluated at the disc gives

$$P_a - P_1 = 2U_d(U_d - 1)$$

2.24

2.3.1.2.  $X \geq 0$  -- OUTFLOW. The inviscid one-dimensional momentum equation for outflow

$$dP = -2UdU \quad 2.25$$

shows  $dP/dU$  to be negative for all values of  $U$ . This means that  $dP$  and  $dU$  are of opposite sign. Outflow of an incompressible fluid from a constant area tube dictates that  $dU$  must be negative, hence  $dP$  must be positive. A positive  $dP$  means either: (1)  $P_2 < P_a$  which is not compatible with outflow or (2)  $P$  increases with  $X$  behind the actuator disc. Case (2) must also be ruled out since the porous walls cannot sustain a pressure difference and outflow results in a continual pressure rise. Thus outflow cannot exist behind the actuator disc for an inviscid flow. Therefore, the pressure can only be atmospheric everywhere behind the disc and the velocity remains constant at the value through the disc,  $U_d$ . The flow situation for an inviscid fluid is depicted in Fig. 2.

2.3.1.3. Thrust. The thrust of the actuator disc is equal to the pressure jump across the disc times the disc area, thus

$$T = (P_a - P_1) \alpha$$

In non-dimensional form the thrust coefficient, defined as

$$C_T \equiv T / \frac{1}{2} \rho U_w^2 \alpha$$

becomes

$$C_T = P_a - P_1 = 2U_d(U_d - 1)$$

2.26

after solving for  $P_a - P_1$  from eq. 2.24.

### 2.3.2. Viscous Flow

2.3.2.1.  $X \leq 0$  -- INFLOW. For  $U \geq 1$ , the friction term is negative, i.e. the flow is moving faster than the wall, hence the viscous effect has a tendency to retard the flow. Equation 2.1, repeated here for ease of reference,

$$dP = -2(2U-1) dU + 2C_T(1-U)/1-U dX \quad 2.1$$

shows  $dP \leq 0$  for all  $U \geq 1$  since  $dU > 0$  for inflow.

As an approximation, the inviscid velocity distribution may be used for the viscous case with substitution for  $U$  and  $dU$  in eq. 2.1.

$$U = \frac{1}{2} \left[ 1 + \cosh(\lambda'X + C_2) \right] \quad 2.22$$

$$dU = \frac{\lambda'}{2} \sinh(\lambda'X + C_2) dX$$

Integrating and evaluating between  $X_0$  and  $X$  yields

$$\begin{aligned} P_a - P &= \frac{1}{2} \left[ \cosh^2(\lambda'X + C_2) - 1 \right] \\ &+ \frac{C_T}{\lambda} \left[ \frac{3}{4} \left( X + \frac{C_2}{\lambda} \right) - \sinh(C_2) + \frac{1}{8} \sinh(2C_2) \right] \end{aligned} \quad 2.27$$

For  $X = 0$ , eq. 2.27 gives the approximate pressure immediately ahead of the disc as

$$P_a - P_1 = 2U_d(U_d - 1) + \frac{C_T}{\lambda} \left[ \frac{3}{4} C_2 - \sinh(C_2) + \frac{1}{8} \sinh(2C_2) \right] \quad 2.28$$

In eqs. 2.27 and 2.28, the first terms represent the change in momentum for inviscid flow. The second terms represent the viscous effects which are dependent upon both the friction factor and the wall porosity.

Equation 2.28 gives an approximate value of  $P_a - P_1$  for a given  $U_d$  to use as initial values for the numerical solution of eqs. 2.1 and 2.2.

For the final solution an iterative procedure must be used to determine the correct value of  $P_a - P_1$  such that the up-stream boundary conditions of  $P_a - P = 0$  and  $U = 1$  are satisfied simultaneously.

2.3.2.2.  $X \geq 0$  -- OUTFLOW. Outflow is required behind the actuator disc in order to eventually bring the flow to rest relative to the tube wall. This means  $dP/dU$  must be positive since both  $dP$  and  $dU$  must be negative. Equation A-5 from the Appendix,

$$\frac{dP}{dU} = -2U - \frac{2C_T}{\lambda} \frac{(1-U)|1-U|}{\sqrt{P-P_a}} \quad A-5$$

for  $U \geq 1$ , shows that  $dP/dU$  is positive only if the friction term is greater than the momentum term. Also,  $dP/dU$  is zero for

$$\sqrt{P-P_a} = -\frac{C_T}{\lambda} \frac{(1-U)|1-U|}{U}$$

which shows  $P - P_a = 0$  when  $U = 1$ . Again, numerical solutions and an iteration procedure are required to determine  $P_2 - P_a$ .

2.3.2.3. Thrust. The thrust coefficient for the actuator disc with viscous flow is given by

$$C_T = P_2 - P_1 = P_2 - P_a + P_a - P_1$$

#### 2.4. The Vehicle as Matched Drag and Actuator Discs

For a fluid-supported internally-propelled vehicle, the resistance consists entirely of aerodynamic drag. Thus, for steady level motion, there can be no unbalanced aerodynamic force on the vehicle, i.e., the thrust must equal the drag. Therefore, in the vehicle frame of reference, the stream force ahead of the vehicle must equal the stream force behind the vehicle less any increase in momentum due to inflow over the length of the vehicle.

2.4.1. Drag - Actuator Disc Combination. The internally propelled vehicle can be represented by a drag disc followed by (an appropriate distance away) an actuator disc matched to give a thrust equal to the drag. The drag disc will cause a pressure rise hence outflow and a decrease in velocity in the region ahead of itself. The actuator disc operates in the wake of the drag disc, thus is affected by and in turn influences the flow through the drag disc. Inflow must occur in the region between the discs as the actuator disc accelerates the flow to obtain the thrust. It has already been shown that the pressure must be atmospheric behind the actuator disc for inviscid flow. Figure 3 shows schematically the model with the expected pressure and velocity distributions.

The equations already developed for the drag and actuator discs alone still apply but must be matched through the new boundary conditions. Using the notation of Fig. 3 and considering inviscid flow, the

appropriate relations for the drag disc are

$$P_1 - P_a = 1 - U_d^2 \quad 2.4$$

$$P_1 - P_2 = U_d^2 \left( \frac{1}{\beta^2} - 1 \right) \quad 2.12$$

$$P_2' - P_2 = 2U_d^2 \left( \frac{1}{\beta} - 1 \right) \quad 2.15$$

For the inflow region ahead of the actuator disc, the momentum equation (eq. 2.7), integrated from  $P_3$  and  $U_3$  forward, gives

$$P - P_3 = 2 \left[ U_3^2 - U_3 + U - U^2 \right] \quad 2.29$$

When  $U = U_d$ ,  $P = P_2'$ , and eq. 2.29 becomes

$$P_2' - P_3 = 2 \left[ U_3^2 - U_3 + U_d - U_d^2 \right] \quad 2.30$$

Setting the thrust equal to the drag yields

$$P_a - P_3 = P_1 - P_2' \quad 2.31$$

since  $P_4 = P_a$ . When the stream force ahead of the vehicle is equated to the stream force behind the vehicle less the increase in momentum due to inflow along the vehicle, the following equation results

$$p_1 \alpha + \rho \alpha U_d^2 = p_4 \alpha + \rho \alpha U_3^2 - \rho \alpha U_w (U_3 - U_d)$$

or, in normalized form,

$$P_1 - P_a = 2 \left[ U_3^2 - U_3 + U_d - U_d^2 \right] \quad 2.32$$

Equations 2.30, 2.31 and 2.32 are not all independent, hence one more equation is needed - the integrated continuity equation for inflow between the two discs. Equation 2.29, rearranged gives  $P_a - P$  as

$$P_a - P = P_a - P_3 + 2 \left[ U^2 - U + U_3 - U_3^2 \right]$$

and substitution into the inflow continuity equation for  $P_a - P$  gives

$$\frac{dU}{\sqrt{U^2 - U + U_3 - U_3^2 + \frac{P_a - P_3}{2}}} = \lambda' dX$$

Integrating and rearranging to obtain U explicitly, yields

$$U = \frac{1}{B} \left\{ \left( \frac{1}{4} - C \right) e^{-\lambda' X} + \frac{B}{2} + \frac{B^2}{4} e^{\lambda' X} \right\} \quad 2.33$$

where

$$C = U_3 - U_3^2 + \frac{P_a - P_3}{2}$$

and

$$B = 2U_3 - 1 + 2 \sqrt{\frac{P_a - P_3}{2}}$$

At  $X = L$ ,  $U = U_d$  and eq. 2.33 can be solved for  $P_a - P_3$ . Thus

$$\begin{aligned}
P_a - P_3 &= 2 \left[ \frac{1}{-4 \sinh(-\lambda' L)} \left( 2U_d - 1 - (2U_3 - 1) e^{\lambda' L} \right. \right. \\
&\quad \left. \left. \pm \left\{ \left[ (2U_3 - 1) e^{\lambda' L} - (2U_d - 1) \right]^2 - 4 \sinh(-\lambda' L) \left[ (2U_d - 1)(2U_3 - 1) \right. \right. \right. \right. \\
&\quad \left. \left. \left. - (2U_3 - 1)^2 \cosh(-\lambda' L) \right] \right\}^{\frac{1}{2}} \right) \right]^2
\end{aligned} \tag{2.34}$$

Equating eqs. 2.4 and 2.32 yields

$$U_3 = \frac{1}{2} \left[ 1 \pm \sqrt{1 + 2(U_d - 1)^2} \right] \tag{2.35}$$

Because of the nature of the above equations, a solution is best obtained by specifying  $U_d$  and solving for the remaining terms, including  $\beta$ . Equation 2.35, for a specified value of  $U_d$ , gives  $U_3$ . In turn, eqs. 2.34, 2.30 and 2.4 give  $P_a - P_3$ ,  $P_2 - P_3$ , and  $P_1 - P_a$ . Equations 2.31, 2.12 and 2.15 can be solved for  $\beta$  as

$$\beta = \frac{1}{1 - \phi} \left[ 1 \pm \sqrt{\phi} \right] \tag{2.36}$$

where

$$\phi = P_1 - P_2' / U_d^2$$

Thus the entire flow field is specified for the case of matched internal propulsion. The drag, and consequently the thrust required, are dependent upon the product of the wall porosity and the vehicle length for lengths up to a critical length,  $X_o$ . For lengths greater than  $X_o$ , the disc conditions of  $U_d$ ,  $\beta$ , and  $C_D$  are independent of the actuator disc.  $X_o$  is determined from eq. 2.33 for  $U = U_d$  and  $P_a - P_3 = P_1 - P_2'$ , with  $P_1 - P_2'$  evaluated for the drag disc alone and for the same  $U_d$ . Thus  $X_o$  is given by

$$X_o = \frac{1}{\lambda} \ln \left[ \frac{2U_d - 1 + 2\sqrt{U_d^2 - U_d + U_3 - U_3^2 + \frac{P_1 - P_2'}{2}}}{2U_3 - 1 + 2\sqrt{\frac{P_1 - P_2'}{2}}} \right] \quad 2.37$$

2.4.2. Actuator - Drag Disc Combination. An internally propelled vehicle may also be simulated by an actuator disc followed by (an appropriate distance away) a drag disc. This configuration, with the thrust generator located at the front of the vehicle, might be superior from the standpoint of reducing the effects of choking in a non-porous tube.

Ahead of the actuator disc, the pressure decreases and the velocity increases as for the actuator disc alone. Thus the momentum equation for inflow gives, using the previously defined notation,

$$P_a - P_3 = 2 \left[ U_3^2 - U_3 \right] \quad 2.38$$

Between the actuator and drag discs, (from 4 to 1) the pressure will increase causing outflow and a decrease in velocity. The pressure will then drop across the drag disc. As previously determined for the drag disc alone, the pressure behind the drag disc must be atmospheric unless the velocity through the disc is less than one half. For reasonable blockage ratios, the velocity will be greater than one half so  $P_{2'} = P_a$ .

The thrust must equal the drag, hence

$$P_4 - P_3 = P_1 - P_a \quad 2.39$$

Also, the stream force ahead of the actuator disc (at 3) must equal the stream force behind the drag disc (at 2') plus the momentum decrease due to outflow from 3 to 2'. Thus

$$P_3 \alpha + \rho \alpha U_3^2 = \rho \alpha \int_{U_3}^{U_d} U dU + P_a \alpha + \rho \alpha U_d^2$$

or

$$P_a - P_3 = U_3^2 - U_d^2 \quad 2.40$$

Outflow occurs from 4 to 1 between the discs, and the integrated outflow momentum equation yields

$$P - P_a = P_1 - P_a + U_d^2 - U^2$$

Substitution for  $P - P_a$  in the outflow continuity equation gives

$$\frac{dU}{\sqrt{-U^2 + U_d^2 + (P_1 - P_a)}} = -\lambda dX$$

and integration from the drag disc ( $X = 0$ ) forward yields

$$U = \sqrt{U_d^2 + (P_1 - P_a)} \sin(-\lambda X + C_3) \quad 2.41$$

where

$$C_3 = \sin^{-1} \left( \frac{U_d}{\sqrt{U_d^2 + (P_1 - P_a)}} \right)$$

At  $X = L$ ,  $U = U_3$  and eq. 2.41 can be rearranged to give

$$P_1 - P_a = \frac{U_3^2}{\sin^2(-\lambda L + C_3)} - U_d^2 \quad 2.42$$

or solving for the length  $L$

$$L = \frac{1}{-\lambda} \left[ \sin^{-1} \frac{U_3}{\sqrt{U_d^2 + (P_1 - P_a)}} - \sin^{-1} \frac{U_d}{\sqrt{U_d^2 + (P_1 - P_a)}} \right] \quad 2.43$$

Equation 2.41 cannot be solved for  $P_1 - P_a$  explicitly since  $C_3$  is also a function of  $P_1 - P_a$ .

A critical length exists such that

$$\sin(-\lambda L_c + C_3) = 1$$

which leaves for all lengths greater than the critical

$$P_1 - P_a = U_3^2 - U_d^2 \quad 2.44$$

which is of course, equal to the thrust,  $P_a - P_3$ . The critical length is given by

$$L_c = \frac{\pi/2 - C_3}{-\lambda} \quad 2.45$$

Equations 2.12 and 2.15 still apply for the drag disc and when combined yield

$$P_1 - P_a = \frac{U_d^2}{\beta^2} (1 - 2\beta + \beta^2) \quad 2.46$$

or, solving for  $\beta$ , gives

$$\beta = \frac{1}{1 - \phi} \left[ 1 \pm \sqrt{\phi} \right] \quad 2.47$$

where

$$\phi = P_1 - P_a / U_d^2$$

Equating eqs. 2.38 and 2.40 gives  $U_3$  as

$$U_3 = 1 \pm \sqrt{1 - U_d^2} \quad 2.48$$

The positive root is required since  $U_3 \geq 1$ .

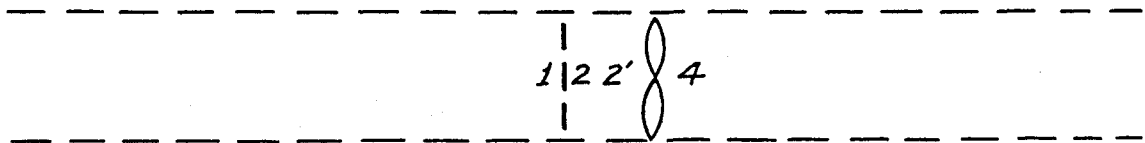
A solution for a vehicle of a given blockage and length is involved and requires a number of estimations and iterations. Solving eq. 2.45 for  $\phi$  in terms of  $\beta$  gives

$$\phi = \left( \frac{1 - \beta}{\beta} \right)^2 \quad 2.49$$

which then permits specifying  $\beta$ . Then from the definition of  $\phi$  and an assumed value of  $U_d$ ,  $P_1 - P_a$  can be calculated. For the assumed  $U_d$ , eq. 2.48 gives the value of  $U_3$ . The corresponding length required can then be obtained from eq. 2.43. A number of trials may be necessary to obtain the required  $U_d$  to satisfy the specified length.

Once the correct values of  $U_d$  and  $P_1 - P_a$  are determined,  $P_a - P_3$  can be calculated from eq. 2.38 and the entire flow field is determined.  $P_1 - P_a$  represents the drag of the vehicle and as such is dependent upon the wall porosity, and the vehicle length and blockage.

2.4.3. Doublet. A doublet, defined as the limiting case of a drag disc and an actuator disc at a zero distance apart, is shown schematically below.



There is no inflow or outflow between the discs, however, the flow is assumed to accelerate through the drag disc and expand back to fill the tube at 2' before entering the actuator disc. In the notation of the drag disc, stations 2' and 3 are coincident.

With no inflow between the two discs, the stream force at 1 must equal the stream force at 4 for the thrust to equal the drag. Thus for incompressible flow with the mass flow rates at 1 and 4 equal, the pressures at 1 and 4 must also be equal. Previously, it was shown that the pressure must be atmospheric behind the actuator disc (i.e.  $p_4 = p_a$ ),

therefore  $p_1$  also equals  $p_a$  which further requires that  $u_1 = u_d = u_w$ .

This is possible under two conditions. One is the trivial case of

$\beta = 1$  and thus no drag or thrust. The second possibility is that for

a given  $\beta$ ,  $p_1$  and  $p_2$ , adjust such that  $u_1 = u_d = u_w$  and  $p_1 = p_a$ .

The Bernoulli equation from 1 to 2 gives

$$p_1 + \frac{1}{2} \rho u_d^2 = p_2 + \frac{1}{2} \rho \left( \frac{u_d}{\beta} \right)^2$$

or in non-dimensional form with  $p_1 = p_a$  and  $u_d = u_w$

$$P_a - P_2 = \left( \frac{1}{\beta^2} - 1 \right) \quad 2.50$$

Equation 2.50 is the same as eq. 2.12 with  $P_1 = P_a$  and  $U_d = 1$ . The

momentum equation from 2 to 2', assuming no inflow, yields from eq. 2.13

for  $U_d = 1$

$$P_2' - P_2 = 2 \left( \frac{1}{\beta} - 1 \right) \quad 2.51$$

The drag of the doublet, hence the thrust, is the pressure difference

across the drag portion of  $P_a - P_2$ , which, from the above two equations

becomes

$$C_D = \left( \frac{1 - \beta}{\beta} \right)^2 \quad 2.52$$

If the actuator disc is placed ahead of the drag disc, then

the pressure behind the actuator disc must be greater than atmospheric

to produce the thrust. Behind the drag disc, the pressure must also be

atmospheric and the velocity equal to the remote velocity in order for

the stream force to be equal across the doublet. Thus the rise in

pressure behind the actuator disc (the thrust) is equal to the drop in pressure to atmospheric behind the drag disc (the drag).

Using the same notation of 1, 2, and 2' for the drag disc, the pressure  $p_1$  must be greater than atmospheric and is given by

$$P_1 - P_2 = \left( \frac{1}{\beta^2} - 1 \right)$$

The momentum equation from 2 to 2' is, for  $p_{2'} = p_a$

$$P_a - P_2 = 2 \left( \frac{1}{\beta} - 1 \right)$$

and combined, the drag coefficient  $C_D$  becomes

$$C_D = \left( \frac{1 - \beta}{\beta} \right)^2$$

Thus the drag of the doublet is the same whether the actuator disc is ahead of or behind the drag disc. The pressure differences are of the same magnitude for the two cases but the pressure is greater than atmospheric for the case of the actuator disc followed by the drag disc.

It should be noted that the drag is independent of the wall porosity for the doublet.

### 3. EXPERIMENTAL APPARATUS AND PROCEDURE

Experiments were conducted for two purposes: first, to determine the aerodynamic characteristics of perforated walls under the conditions of axial flow through the tube; and second, to verify the theoretical results for the drag disc simulation of the externally propelled vehicle in a perforated-wall tube.

#### 3.1. Aerodynamic Characteristics of Perforated Tubes

3.1.1. Experimental Facility. Tests were conducted to determine the aerodynamic characteristics of perforated walls in the simple set-up shown schematically in Fig. 4. The facility consists of a 3-foot section of 4 inch I.D. plexiglass and 17 feet of 4 inch I.D. aluminum tubing. The plexiglass portion, located between sections of the aluminum tubing, was perforated with 12 circumferential rows, 2 inches apart, of 8 equally spaced  $1/8$  inch dia. holes. Some of these holes were covered with Mystic tape to reduce the porosity. The holes were later enlarged to  $1/4$ ,  $7/16$  and  $5/8$  inches as a means of increasing the wall porosity.

An orifice plate, located up-stream of the perforated section, was used to measure the total flow rate from the pressure chamber. A calibrated flow nozzle, inserted into the open end of the aluminum tube was used to meter the flow rate axially out of the tube. The difference between these two measured values is the volume flow rate through the porous wall section. Static pressure taps are located adjacent to and either side of the perforated portion. These pressure taps, each

connected to one side of a U-tube water manometer, give the pressure difference across the tube wall directly.

The rotary air compressor, driven by a variable speed electric motor, supplies air continuously to the pressure chamber. The volume flow rate through the tube was controlled by the speed of the compressor and by the control valve at the exit of the pressure chamber.

For the arrangement shown in Fig. 4, the pressure in the tube was greater than atmospheric and outflow through the tube wall occurred. For inflow tests, the inlet to the pressure chamber was attached to the inlet to the rotary compressor and the air drawn in through the tube walls and through the tube itself. For these inflow tests, the nozzle and orifice plate was reversed.

3.1.2. Test Procedure. The orifice plate was calibrated with a standard calibration nozzle for the entire range of compressor speeds by inserting a solid section of plexiglass tubing and metering the flow. Then with 1/8 inch dia. holes in the perforated section and the apparatus arranged for outflow as shown in Fig. 4, tests were run for a range of motor speeds of 600 to 1400 RPM. This provided a range of volume flow rates of from 25 to 60 cfm through the orifice plate and corresponding tube axial velocities of the order of 10 fps. Manometer readings were taken for the orifice plate, tube wall pressure taps and the nozzle along with the atmospheric pressure and flow temperature readings. The holes were then covered with tape, one row at a time, and the readings taken again. The apparatus was changed over for inflow and the tests repeated for the same hole size. Next, the diameter of the holes was increased

consecutively, to 1/4, 7/16 and 5/8 inches and the entire procedure repeated.

3.1.3. Data Reduction. The tube axial velocity,  $V_T$  and the corresponding dynamic pressure,  $q_T$  were determined from the volume flow rate through the orifice plate, the tube cross-sectional area, and the local temperature and pressure as expressed by

$$V_T = \dot{Q}_{\text{ORIFICE}} / \text{Tube Area}$$

$$q_T = \frac{1}{2} \rho V_T^2$$

The volume flow rate through the porous wall was calculated as the difference between the flow rates through the orifice and the nozzle. The average velocity through each hole in the wall,  $V_w$  was then obtained by the relations

$$\dot{Q}_{\text{WALL}} = \dot{Q}_{\text{ORIFICE}} - \dot{Q}_{\text{NOZZLE}}$$

$$\frac{V_w}{V_T} = \frac{\dot{Q}_{\text{WALL}} / \text{AREA OF HOLES}}{V_T}$$

The pressure difference across the wall that causes the inflow or outflow, was taken to be the average of the two static pressure readings up-stream and down-stream of the perforated section as given by

$$\frac{\Delta P_w}{q_T} = \frac{(\Delta P_1 + \Delta P_2)}{2 q_T}$$

Some of the above tests were repeated in a second similar facility capable of greater flow rates. This facility, described below,

was constructed for the purpose of extending the range of tests and for testing the drag disc in a porous tube. This second facility has the capacity of 600 cfm which gave axial velocities in the order of 100 fps in a 4 inch dia. tube.

### 3.2. Drag Disc in a Perforated-Wall Tube

3.2.1. Experimental Facility. The existing laboratory facility for flow measurement experiments consisting of a centrifugal blower, 7-5/8 inch dia. steel duct and installed flow metering devices, was modified by removing a portion of the ducting and all of the meters except the venturi. A reducer was made to accommodate 4 inch I.D. plexiglass tubing. The plexiglass tubing was uniformly perforated, as previously described, over the entire length of the two 4-foot sections. Discs of various porosities were installed perpendicular to the tube axis between the two perforated plexiglass sections and taped in place. Twelve pressure taps were installed in the porous sections for measurement of the pressure difference across the tube wall.

A schematic of this facility is shown in Fig. 5. Figure 6a is a photograph of the entire facility while Fig. 6b is a close-up of the porous tube in the vicinity of the perforated disc.

3.2.2. Test Procedure. Tests were conducted by inserting a particular drag disc between the two perforated sections and for a given setting of the damper control valve, manometer readings were taken for each pressure tap along the tube and for the venturi meter. For some tests, pitot-static probe measurements were also made at several axial locations and radially across the tube. Some variation in volume flow

rates was obtained by adjusting the control valve and new readings were made. Discs of different porosities were then tested for the same tube wall porosity, then the procedure was repeated for increased hole sizes to give larger porosities.

3.2.3. Data Reduction. The axial dynamic pressure,  $q_T$  was calculated from the measured volume flow rate through the venturi meter and the corresponding measured pressure and temperature. This dynamic pressure, plus the static pressure measured at the entrance to the perforated section gives the entrance total pressure. The normalizing remote velocity,  $V_i$ , was taken as the velocity that would exist for that total pressure, if the static pressure were expanded isentropically to atmospheric pressure.

The normalized pressure difference across the wall,  $P - P_a$ , was calculated as the measured static pressure divided by the remote dynamic pressure,  $q_i$ . The local axial velocity was determined from the pitot-static probe measurements and the local static pressure and normalized by the remote velocity,  $V_i$ .

#### 4. DISCUSSION OF RESULTS

Solutions to the equations of motion governing the flow field induced by a vehicle traveling through an infinitely long porous tube represent a two-point boundary value problem. The flow is known to be at rest far up-stream and far down-stream of the vehicle, at least for viscous flows. Solution of these equations, however, requires a numerical integration technique because of their complexity. Furthermore, solutions must be obtained for each region and then matched at the interface between regions, i.e., at the vehicle.

Numerical solutions have been obtained using a Runge-Kutta forward integration scheme to solve the momentum and continuity equations simultaneously. This technique requires knowing initial values for pressure and velocity and integrating with respect to distance. Inviscid flow closed-form solutions have been obtained which permit the determination of the disc conditions for a specified drag disc porosity or actuator disc thrust. For viscous flow, however, closed form solutions are not possible and an iterative scheme is required to determine the correct disc conditions which satisfy the up-stream and down-stream boundary conditions.

The assumption has been made that the velocity through the wall is proportional to the square root of the pressure difference across the wall as given by eq. 2.3. Figure 7 shows the results of test conducted to verify this assumption. As presented, the test data exhibits a straight line trend, the slope of which is the value of the flow coefficient,  $C_f$  in eq. 2.3, thus verifying the assumed form of the velocity function.

All of the data points for inflow appear to lie on the same straight line through the origin corresponding to a flow coefficient of  $C_f = .75$ . For outflow, two curves of different slopes are evident. The steeper curve corresponds to  $C_f = .60$  and represents data for relatively low axial flow velocities ( $V_T = 10$  fps). The flagged data, corresponding to  $C_f = .9$ , represents data for axial flow velocities of the order of 100 fps. A stagnation point exists on the downstream portion of each hole due to the turning of the flow to go through the wall. Thus the higher axial velocity in the tube results in a higher velocity through the wall for a given static pressure difference across the wall. Furthermore, when the tube wall thickness is of the same order as the hole diameter, a somewhat irregular and non-linear pressure drop occurs through the wall<sup>10</sup>.

All results are presented in a normalized form with pressures given as the difference between the local static pressure and atmospheric pressure. A constant value of  $C_f = .65$  for inflow and outflow has been used for all of the theoretical calculations throughout this investigation.

#### 4.1 The Vehicle as a Drag Disc

For inviscid flow, eqs. 2.14 or 2.16 are used to determine the mass flow velocity,  $U_d$  through the disc for a specified value of disc porosity,  $\beta$ . For  $U_d \geq .5$ , the pressure is atmospheric in the flow region behind the disc and no inflow occurs, thus eq. 2.14 applies. Equation 2.16 applies for  $U_d \leq .5$  which means that inflow occurs behind the drag disc. Figure 8 shows the velocity through the disc as a function of disc porosity for both inviscid and viscous flows.

The viscous flow solution is for a tube-wall friction factor of  $C_f = .01$  and a 2.5 per cent wall porosity. All solutions for larger wall porosities and/or lower friction factors lie between the two curves. Thus very little difference is found in the velocity through the disc for changes in friction factor or wall porosity. The individual points on the graph represent experimental data obtained by Taylor<sup>11</sup> and modified to correspond to the conditions of this analysis.  $\beta$  for the perforated plate, as used by Taylor, is the geometric ratio of the open area to the total area of the disc. For this investigation, however,  $\beta$  is an effective porosity and can be obtained from the solution of the conservation equations. As such,  $\beta$  represents the product of the contraction coefficient,  $C_c$  and the geometric porosity of the disc. Thus for an approximate value for the contraction coefficient based on the results for an orifice plate<sup>12</sup>, excellent agreement is shown between Taylor's results and the results of this investigation.

The pressures ahead of and behind the drag disc are presented as functions of disc porosity in Fig. 9. For inviscid flow, the pressure and velocity at the disc are independent of the magnitude of the wall porosity. For viscous flow, however, the pressure does depend on the magnitude of the wall porosity for values of  $\beta$  less than approximately .6. For larger values of  $\beta$ , there is no perceptible pressure difference across the wall behind the disc and the viscous and non-viscous solutions coincide.

Thus for the drag disc, or simulated externally propelled vehicle, the wall porosity has the greatest effect for the low disc porosities or large vehicle blockage ratios. Furthermore, a large pressure relief is

evident even for wall porosities as low as 1 or 2.5 per cent.

The drag of the disc, given by eq. 2.17, is presented in Figs. 10 and 11 as a function of the disc porosity. Figure 10 shows the drag to decrease for increasing wall porosities for values of  $\beta$  up to about .6. If compressibility is considered, the effect of porous walls would be felt for higher values of  $\beta$ .

Figure 11 shows the drag of the disc for a 2.5 per cent wall porosity and for various values of friction factor.\* As expected, a decrease in friction factor results in a lower value of vehicle drag. In the disc-fixed frame of reference, the effect of viscosity is to increase the stagnation pressure in the direction of the flow due to the moving wall. This causes a higher total pressure at the disc and thus an increased drag of the disc. Experimental data points from ref. 11 are also shown. Again  $\beta$  has been modified to account for flow contraction through the disc. It should be noted that Taylor's results are for perforated plates dropped in open water and not within a porous tube. The drag of a solid plate in the open and normal to the flow has been found to be about  $1.9^{13}$ . All of these measured values of drag tend to confirm the validity of the present analysis.

The total effect of a porous-wall is best shown in Figs. 12, 13, and 14. Figures 12 and 13 present the pressure and velocity distributions as functions of distance from the drag disc for various wall porosities and for both inviscid and viscous flow respectively. Increasing the wall porosity reduces the distance for disturbed flow ahead of the vehicle. For inviscid flow the velocity does not return to the wall velocity behind the drag disc, but instead a constant velocity wake of  $U = U_d$  for

---

\* The friction factor would depend on the wall porosity and on whether for inflow or outflow.

$U_d \geq .5$  and of  $U = .5$  for  $U_d < .5$  is maintained. The effect of viscosity is to bring the flow to rest relative to the wall and a finite length wake results. Frictional effects bring the flow to rest in a distance of about 600 tube diameters ( $X = 1200$ ) for a friction factor of .01. Figure 14 presents the pressure and velocity as functions of distance for a 2.5 per cent wall porosity and for various friction factors. The inviscid solution is also shown for comparison.

Experimental results have been obtained for cases of a stationary wall relative to the drag disc. Pressure was measured by means of static pressure taps at the wall located midway between equally spaced rows of holes. The velocity was determined from pitot-static probe measurements taken along the tube center-line. The pressure and velocity are normalized relative to the dynamic pressure and velocity that would exist at the inlet to the perforated tube if the flow at the inlet was expanded isentropically to atmospheric pressure.

Figures 15 and 16 show the experimental and corresponding theoretical results of pressure and velocity as functions of distance for a wall porosity of 4.8 per cent and for two different porous discs. A flow coefficient,  $C_f = .56$  was assumed based on the experimental distance required for the pressure to reach atmospheric. Figure 15 shows the results for a disc of 50 per cent geometric porosity which resulted in a velocity at the disc  $U_d = .48$  and a pressure ahead of the disc of  $P_1 - P_a = .76$ . Behind the disc there was no measurable pressure difference or velocity change. Modification of the geometric disc porosity by a contraction coefficient of  $C_c = .73$ , gives a value of  $\beta = .365$  which corresponds precisely with the inviscid curve of Fig. 8. The results presented in Fig. 15 show the flow to be disturbed over a distance of

only about 20 tube radii with very good correlation between theory and experiment.

A 1/4" aluminum disc with 1/4" dia. holes ( $\beta_{geo.} = .23$ ), shown in Fig. 19, was tested and the results are shown in Figs. 16 through 18. Figure 16a and 16b show the velocity and pressure distributions as functions of distance. Because of the low value of disc porosity for this test, the pressure is below atmospheric immediately behind the disc. Figure 17 shows the normalized static pressure behind the drag disc as a function of the tube radius indicating a reduced pressure across essentially the full tube diameter. Variations in the pressure are due primarily to the fact that some measurements were taken immediately behind holes and some behind solid portions of the disc. Figure 18 shows a series of velocity profiles, obtained by means of a pitot-static probe, in the vicinity of the disc. The orientation of the velocity traverse is shown in Fig. 19 indicating that the reason for the erratic velocity immediately behind the disc is that two measurements occur directly behind holes in the disc. These results show clearly that the flow is fully expanded and essentially one dimensional within 1 and 1/2 tube diameters behind the drag disc.

Figure 20 shows the variation in the ratio of  $C_{D \text{ viscous}}/C_{D \text{ inviscid}}$  with wall porosity for several values of disc porosity. Recall that the drag coefficient for inviscid flow is not dependent upon the wall porosity as is  $C_{D \text{ viscous}}$ . These curves, generated by cross-plotting the results presented in Fig. 10, show a large decrease in  $C_D$  for even very low values of wall porosity, i.e. for high blockage ratios. A value of  $\beta \geq .5$  would be realistic for a vehicle in a tube, hence wall porosities of only up to 10 per cent would have significant effect. The results

presented in Fig. 20 show the same general trend as the experimental results shown in Fig. 21, which has been reproduced from ref. 9. The experimental results are for an externally propelled vehicle with a 50 per cent blockage ratio and show a significant reduction in the effective drag for porosities up to 10 per cent.

#### 4.2. The Thrust Generator as an Actuator Disc

The actuator disc alone could be considered to represent an internally propelled, wheel supported vehicle with no aerodynamic drag. For such a vehicle, the thrust must balance the rolling resistance only.

The thrust required must be specified for the actuator disc, then for inviscid flow, eq. 2.26 gives the velocity through the disc and the entire flow field can readily be determined. Figure 22 shows the pressure and velocity distributions as functions of distance for various wall porosities and for a constant thrust. Ahead of the disc, the pressure is less than atmospheric causing inflow with a resulting velocity greater than the wall velocity. The distance of disturbed flow decreases with increasing wall porosities. Behind the actuator disc, the pressure is atmospheric and a constant velocity ( $U = U_d$ ) wake is maintained.

Viscous effects are almost negligible as shown by the slight difference in pressure and velocity even for the high friction factor of  $C_f = .02$ , except for the effect of bringing the wake flow to rest relative to the tube walls. The distance required for this viscous dissipation of the wake is large though, being about  $10^4 X$  for a friction coefficient of  $.02$ .

The flow field induced by an actuator disc in a perforated tube is similar to the flow field produced by a propeller in a finite length,

constant area, cylindrical fairing<sup>14</sup>. An actuator disc operating in a finite length constant area fairing produces a low pressure ahead and essentially atmospheric pressure behind the disc. In addition, the flow leaves the fairing in a constant area stream tube with the flow tangent to the exit of the fairing. Like the propeller within a fairing, the actuator disc in a porous-wall tube generates a low pressure region ahead and atmospheric pressure behind the disc with a constant area and constant velocity ( $U = U_d$ ) wake.

An actuator disc without a fairing or shroud, generates a contracting stream tube and a pressure greater than atmospheric immediately behind the disc. This would represent inflow in a region of excess pressure. In the present analysis, as the wall porosity approaches unity, the contracting slip stream is not realized because of the constant area restriction imposed. Furthermore, the analysis shows that the pressure always becomes atmospheric behind the actuator disc. Thus this analysis is not valid in the limit as the wall porosity approaches unity because the flow conditions of the un-shrouded propeller are not satisfied. The extent to which the porosity can be increased is not known.

#### 4.3. The Vehicle as Matched Drag and Actuator Discs

The resistance of a fluid supported internally propelled vehicle is due entirely to aerodynamic drag. Such a vehicle is simulated in this investigation by a combination of a drag disc and an actuator disc. The spacing of these two discs is a measure of the vehicle length while the porosity of the drag disc specifies the effective vehicle

blockage. Frictional drag on the vehicle is not included. Under conditions of level motion, the thrust on the vehicle must equal the drag of the vehicle. For the drag disc followed by the actuator disc, outflow occurs ahead of the drag disc in an amount dependent upon the blockage and the drag. Inflow, in an amount determined by the conservation equations, must occur between the two discs, i.e. over the length of the vehicle.

The results of this analysis for the combined drag and actuator discs are presented in Fig. 23 through 29. The effect of varying the wall porosity is shown in Fig. 23 for a vehicle with a 40 per cent blockage ratio and a length of five times the tube radius. The thrust or drag of the vehicle,  $(P_a - P_3)$  is shown to decrease for increasing porosities up to 10 per cent. For a 10 per cent porosity, the pressure behind the drag disc is atmospheric which is the same as for the drag disc alone. For wall porosities greater than 10 per cent then, the drag remains constant while inflow occurs over less than the full length of the vehicle as shown by the curve for 12.5 per cent. Thus 10 per cent is the critical porosity for the vehicle configuration shown.

It should be noted that the critical wall porosity depends on the vehicle blockage or velocity through the drag disc, and on the corresponding vehicle length. For a vehicle blockage ratio of 1.58 ( $\beta = .60$ ) the critical vehicle length is 10 for a 5 per cent wall porosity while the critical length is 5 for a 10 per cent wall porosity.

The pressure immediately ahead of the drag disc  $(P_1 - P_a)$  increases for increasing porosities up to 10 per cent while the corresponding velocity through the drag disc decreases. For a 12.5 per cent wall porosity, the pressure and velocity at the discs are the same as for a 10

per cent wall porosity but with a further decreased length of disturbed flow ahead of the drag disc. Behind the actuator disc, the pressure is everywhere atmospheric and the wake velocity increases for increased wall porosities. The higher wake velocity is a consequence of the corresponding lower velocity through the drag disc.

Figure 24 shows the effect of viscosity for the case of a 5 per cent wall porosity and a friction coefficient of  $C_f = .01$  which results in a lower velocity through the drag disc and a lower pressure throughout the region between the two discs. The drag is thus increased slightly by the effects of viscosity.

Figure 25 shows the pressure and velocity distributions as functions of distance from the actuator disc for three vehicles of 40 per cent blockage and lengths of 5, 7.5, and 10 times the tube radius and for a wall porosity of 5 per cent. The drag decreases slightly for increasing lengths up to a vehicle length of 10. As the length increases, the velocity through the disc decreases resulting in a higher velocity through the actuator disc. For further increased vehicle lengths, the pressures and velocities would remain as shown for a length of ten.

Figure 26 shows the pressure and velocity distribution for a typical Tubeflight Vehicle as described by Foa<sup>15</sup> and for a 5 per cent porous wall. The vehicle length of 75 ft. and a tube diameter of 15 ft. give a nondimensional length of 10 which is greater than the critical length for the 5 per cent wall porosity. Hence, the pressure is atmospheric and the velocity constant for a short distance behind the drag disc before being influenced by the actuator disc.

Figure 27 shows the comparison of two simulated internally propelled vehicles of 40 per cent blockage and lengths of 5 tube radii with a 5 per cent tube wall porosity. The difference between the two vehicles is the fore or aft location of the thrust generator. The drag is greater for the vehicle with the forward located thrust generator due to the higher velocity through the drag disc.

Figure 28 shows the vehicle drag coefficient as a function of the disc porosity for various wall porosities and for a constant non-dimensional vehicle length of five. Shown also is the curve for the drag disc alone and for a doublet. Increasing the wall porosity reduces the drag of the internally propelled vehicle for blockage ratios greater than 30 per cent and for wall porosities up to about 10 per cent.

It should be noted that the drag disc in all cases simulates a vehicle with flow separation on the after body. This is not unrealistic as the assumption has often been made in the absence of boundary layer control.

Figure 29 shows the vehicle drag coefficient as a function of the wall porosity for a vehicle blockage ratio of 40 per cent and for three different vehicle lengths. The drag coefficient decreases for increasing porosities up to some critical value.

## 5. CONCLUSIONS

This investigation concerns the effects of wall perforations on the performance of both externally and internally propelled tube vehicles.

The results of a one-dimensional analysis show that wall porosity has a beneficial effect on the performance of tube vehicles. The assumption of an incompressible flow limits the validity of the analysis quantitatively - but not qualitatively - to moderate speeds.

Wall perforations have the effect of reducing the effective blockage, hence the drag of the vehicle and the distances ahead of and behind the vehicle where the flow is disturbed. These effects are important for high blockage ratios and become insignificant for blockage ratios below 30 per cent. Changes of wall porosity have a large effect when the wall porosity is very small, and become insignificant when it is greater than about 10 per cent.

For the externally propelled vehicle, properly simulated by the drag disc, the inviscid-flow analysis predicts, in closed-form solutions, a finite-length disturbed flow region ahead and an infinite wake behind the vehicle. In the absence of viscosity, changes of wall porosity modify the distance over which the flow is disturbed but not the maximum amplitude of the disturbances in the tube and the drag of the vehicle. On the other hand, when viscosity is accounted for, the wake is found to return to rest relative to the tube wall behind the vehicle, and the drag is found to be a function of the wall porosity. For large blockage ratios, inflow occurs behind the vehicle regardless of whether the fluid is viscous or not. In contrast, for low blockage ratios, inflow behind the vehicle will take place always and only if the flow is viscous. For wall porosities up to about 10 per cent an increase of porosity causes the

the viscous flow field to diminish in extent and the drag to decrease.

For the internally propelled vehicle, suitably simulated by a drag disc followed by an actuator disc, the overall effect of viscosity is small and the inviscid flow analysis predicts the drag as a function of wall porosity, vehicle length, and blockage. Outflow occurs ahead, inflow over the length, and outflow behind the vehicle. In the region behind the vehicle, the force of the moving wall tends to retard the flow causing an increase in pressure which in turn causes outflow and a gradual return of the flow to ambient conditions and to rest relative to the tube wall.

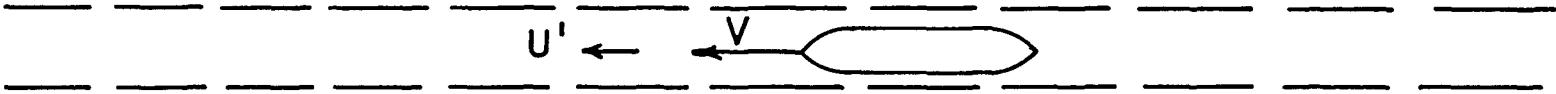
For the model used, the drag of the vehicle is a function of its length up to a critical length which depends on the porosity of the tube wall. A specified amount of inflow is required between the two discs to produce a thrust equal to the drag, hence a lower internal pressure is needed behind the drag disc for a short simulated vehicle to produce this inflow. The lower pressure results in a higher drag. For a vehicle of a given blockage and length, the drag is reduced by increasing the tube wall porosity up to a critical value.

With the forward-located thrust generator, a region of inflow exists ahead, a region of outflow over the length, and in the case of viscous fluids, a region of inflow behind the vehicle. Because of the higher values of velocity at the vehicle, the drag is greater than for a corresponding vehicle with an aft-located thrust generator.

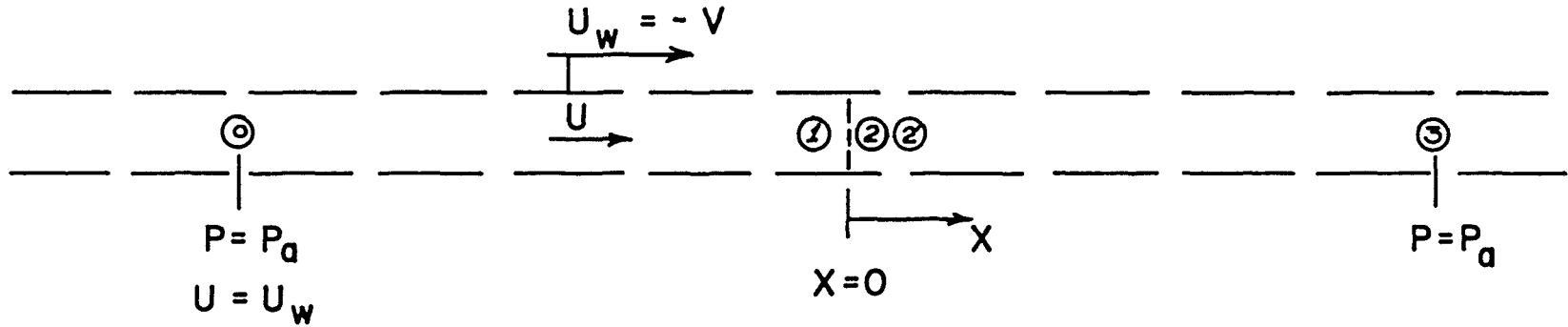
6. REFERENCES

1. Berman, A. S., "Laminar Flow in Channels with Porous Walls," J. Appl. Physics, Vol. 24, 1953, pp. 1232-1235.
2. Sellars, J. R., "Laminar Flow in Channels with Porous Walls at High Suction Reynolds Number," J. Appl. Physics, Vol. 26, 1955, pp. 489-490.
3. Yuan, S. W., "Further Investigation of Laminar Flow in Channels with Porous Walls," J. Appl. Physics, Vol. 27, 1956, pp. 267-269.
4. White, F. M. Jr., B. F. Barfield, and M. J. Goglia, "Laminar Flow in a Uniformly Porous Channel," J. Appl. Mech., Dec. 1958, pp. 613-617.
5. Wageman, W. E., and F. A. Guevara, "Fluid Flow through a Porous Channel," Physics of Fluids, Vol. 3 No. 6, Dec. 1960 pp. 878-881.
6. Friedman, M., and J. Gillis, "Viscous Flow in a Pipe with Absorbing Walls," ASME Paper No. 67 - WA/APM-23.
7. Goodman, T. R., "Aerodynamic Properties of Perforated Walls for use in a Tube Transportation System," Oceanics Technical Report No. 67-39, April 1968 (PB 177766)
8. Foa, J. V., "Power Demands of Tubeflight Vehicles," Rensselaer Polytechnic Institute Tech. Rept. TR AE 6802, January 1968.
9. Cromack, D. E. and Iyer, B., "Experiments on the Propulsion of Vehicles in Tubes of Varying Porosities," Rensselaer Polytechnic Institute, (to be published).
10. Goethert, B. H., Transonic Wind Tunnel Testing, Pergamon Press, New York, 1961, p. 88.
11. Taylor, G. I., and R. M. Davies, "The Aerodynamics of Porous Sheets," Reports and Memoranda No. 2237, April, 1944.
12. Daily, J. W. and Harleman, D. F., Fluid Dynamics, Addison-Wesley Publishing Co. Inc., Reading, Massachusetts (1966) p. 320.
13. Robertson, J. M., Hydrodynamics in Theory and Application, Prentice-Hall, Inc., Englewood Cliffs, N. J. (1965) p. 462.
14. Kuchemann, D. and J. Weber, Aerodynamics of Propulsion, McGraw-Hill Book Co. (1953) p.130.

15. Reference 8, p. 7.
16. Goodman, T.R., "Flow Properties of a Slender Body Traveling Centered in a Perforated Tube," Oceanics Technical Report No. 68-43, April 1968 (PB 177524).

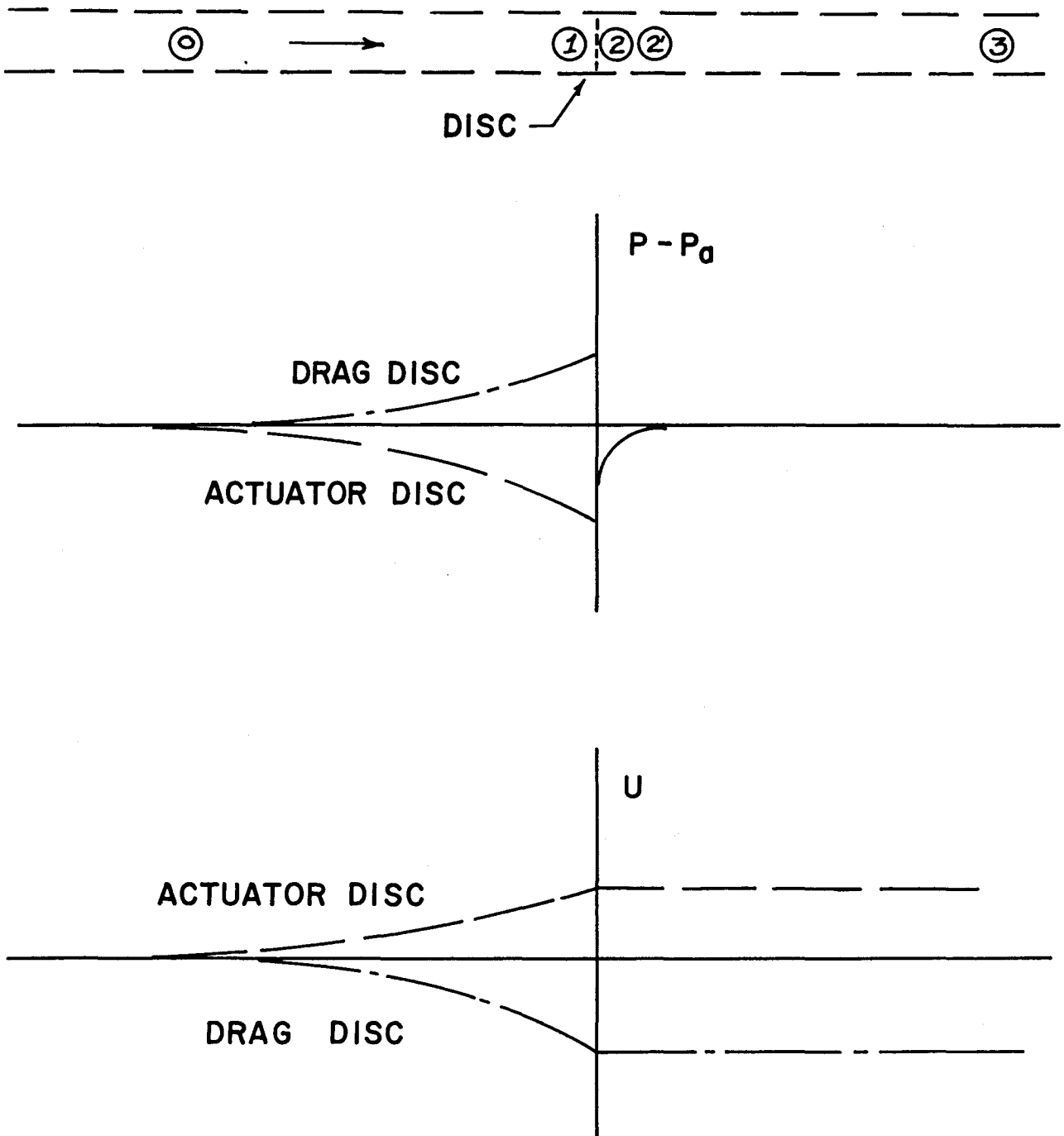


(a) WALL - FIXED FRAME OF REFERENCE



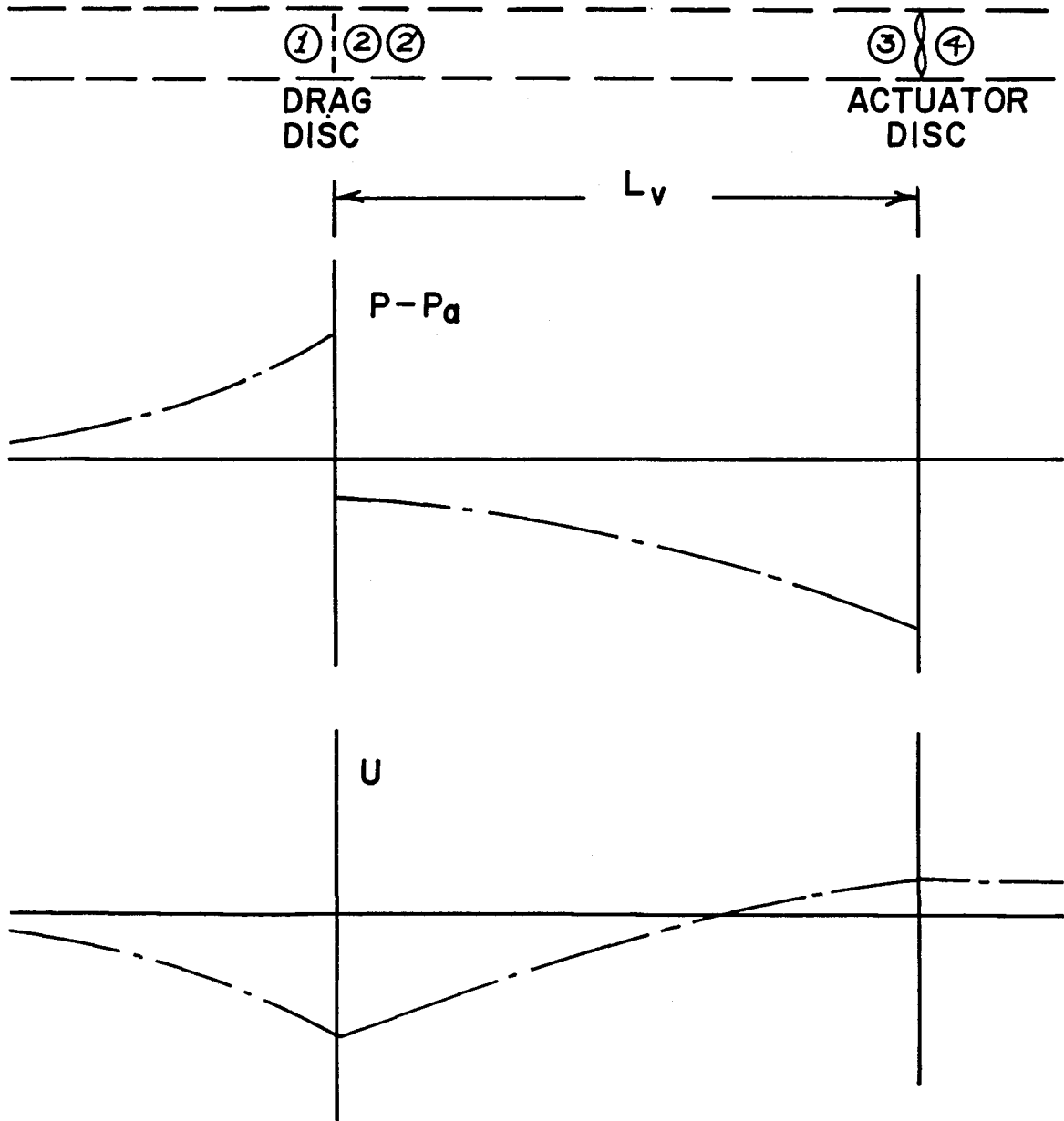
(b) DISC - FIXED FRAME OF REFERENCE

FIGURE I



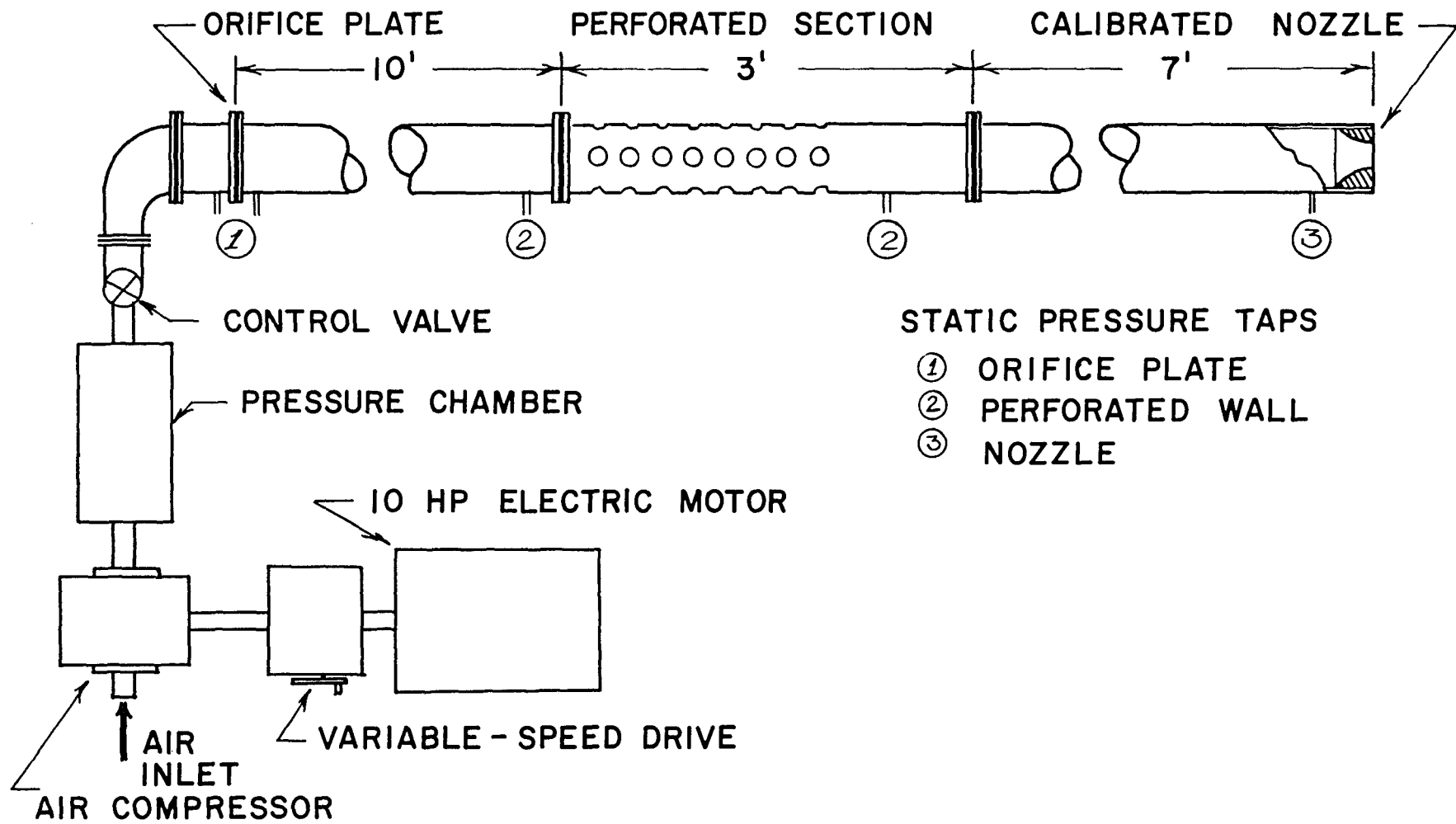
TYPICAL PRESSURE AND VELOCITY DISTRIBUTIONS

FIGURE 2



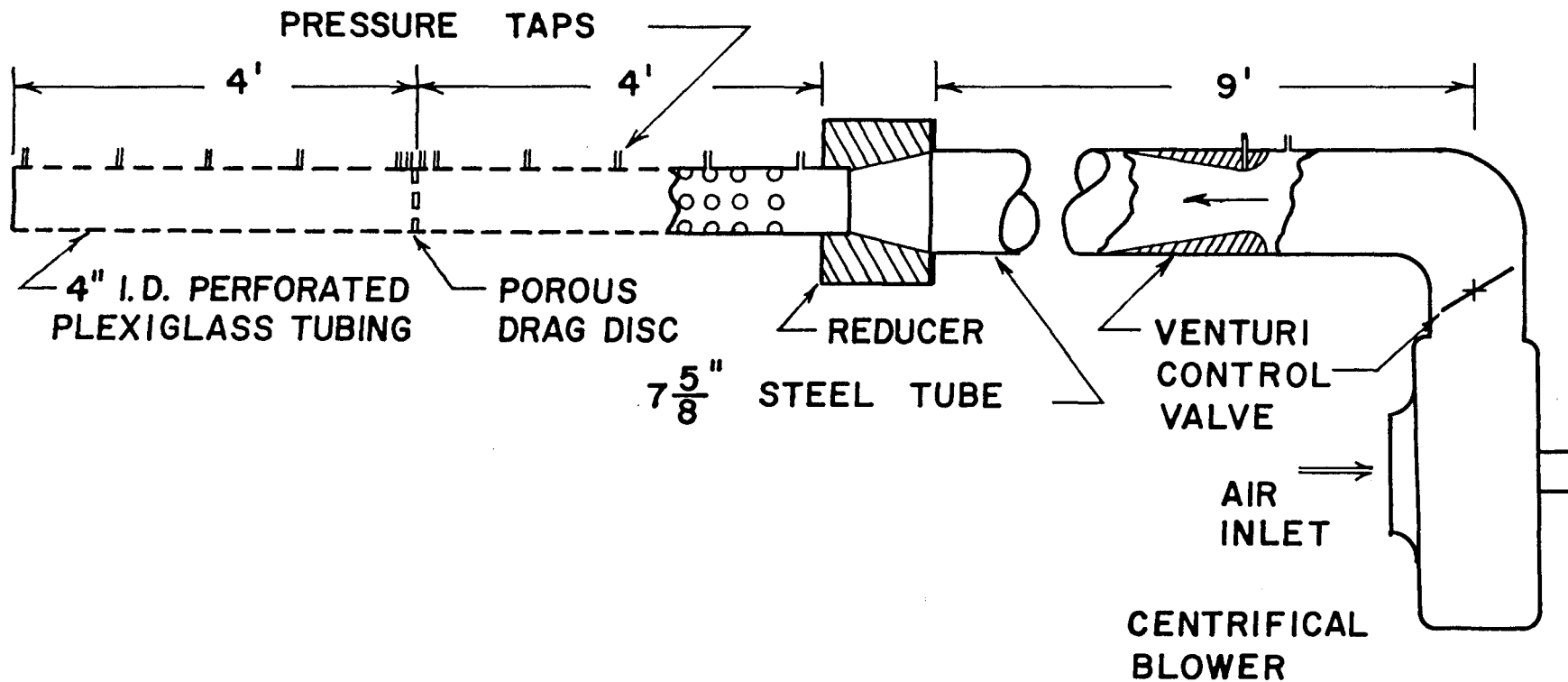
SIMULATED INTERNALLY PROPELLED VEHICLE  
PRESSURE AND VELOCITY DISTRIBUTIONS

FIGURE 3



SCHEMATIC - PERFORATED - WALL TEST FACILITY IN THE  
 MECHANICAL AND AEROSPACE ENGINEERING DEPARTMENT  
 UNIVERSITY OF MASSACHUSETTS

..GURE 4



SCHEMATIC — PERFORATED TUBE — DRAG DISC FACILITY IN THE  
 AERONAUTICAL ENGINEERING DEPARTMENT  
 RENSSELAER POLYTECHNIC INSTITUTE

FIGURE 5

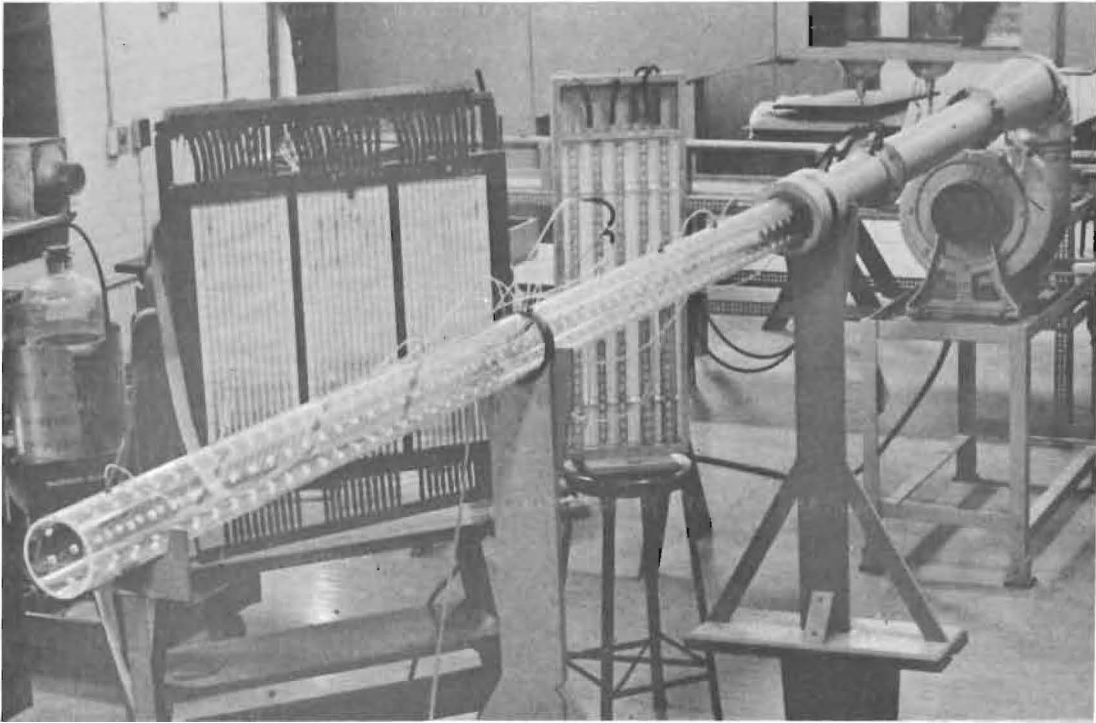


**FIGURE 6a – PERFORATED TUBE-DRAG DISC FACILITY**

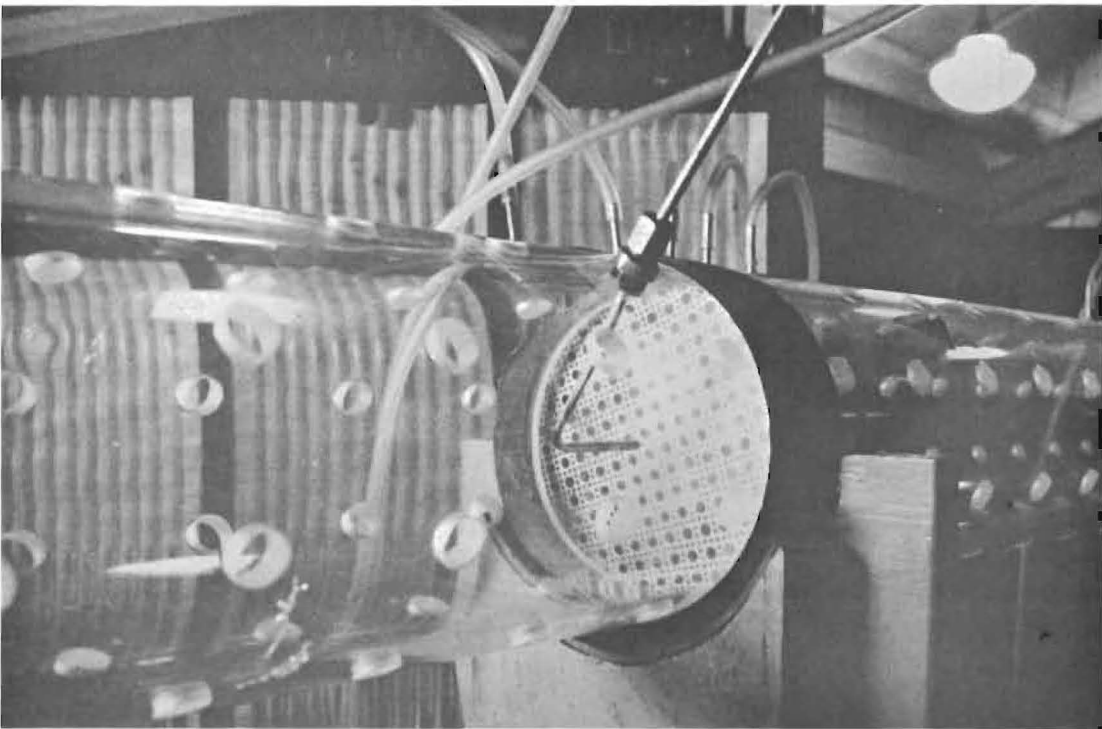
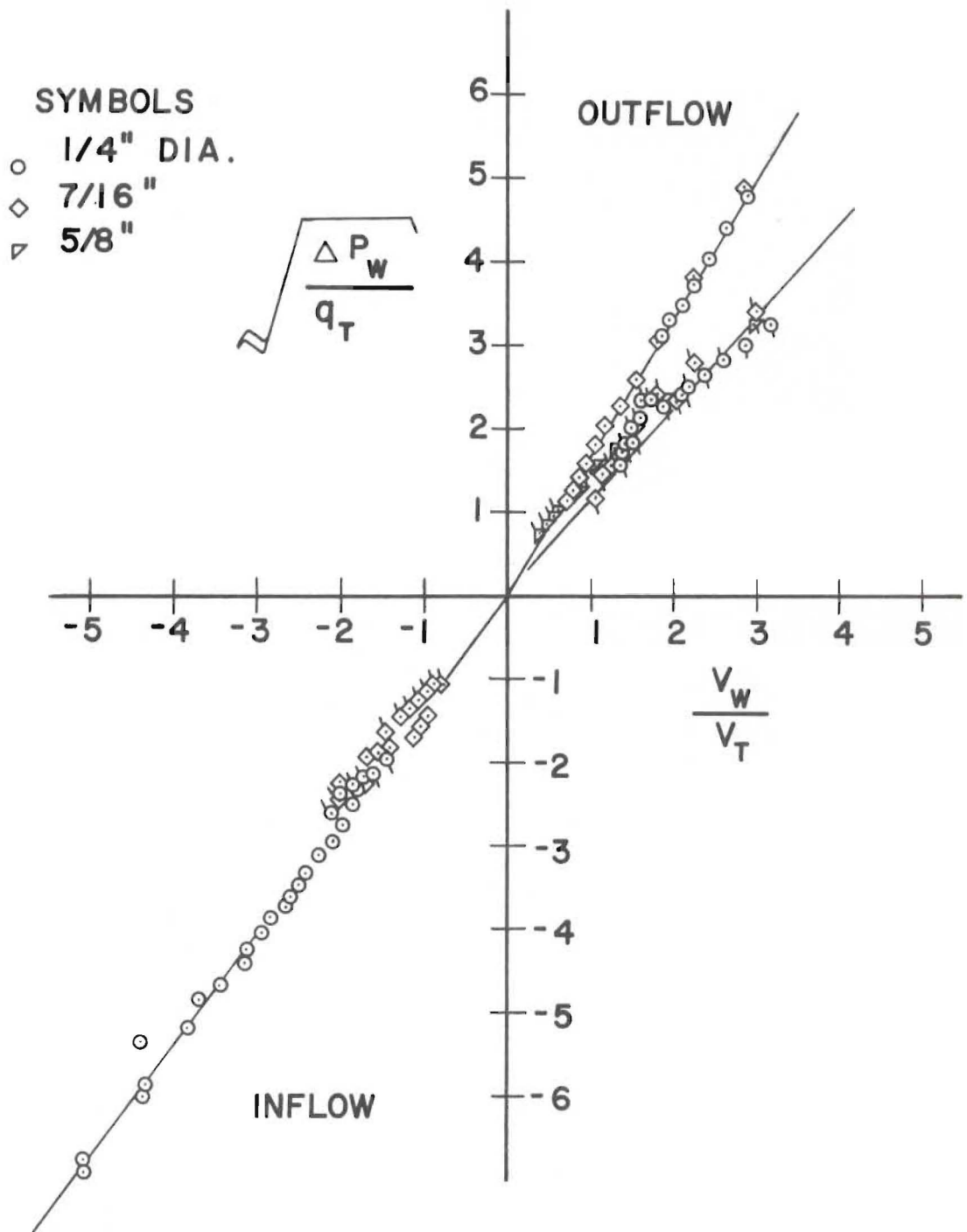


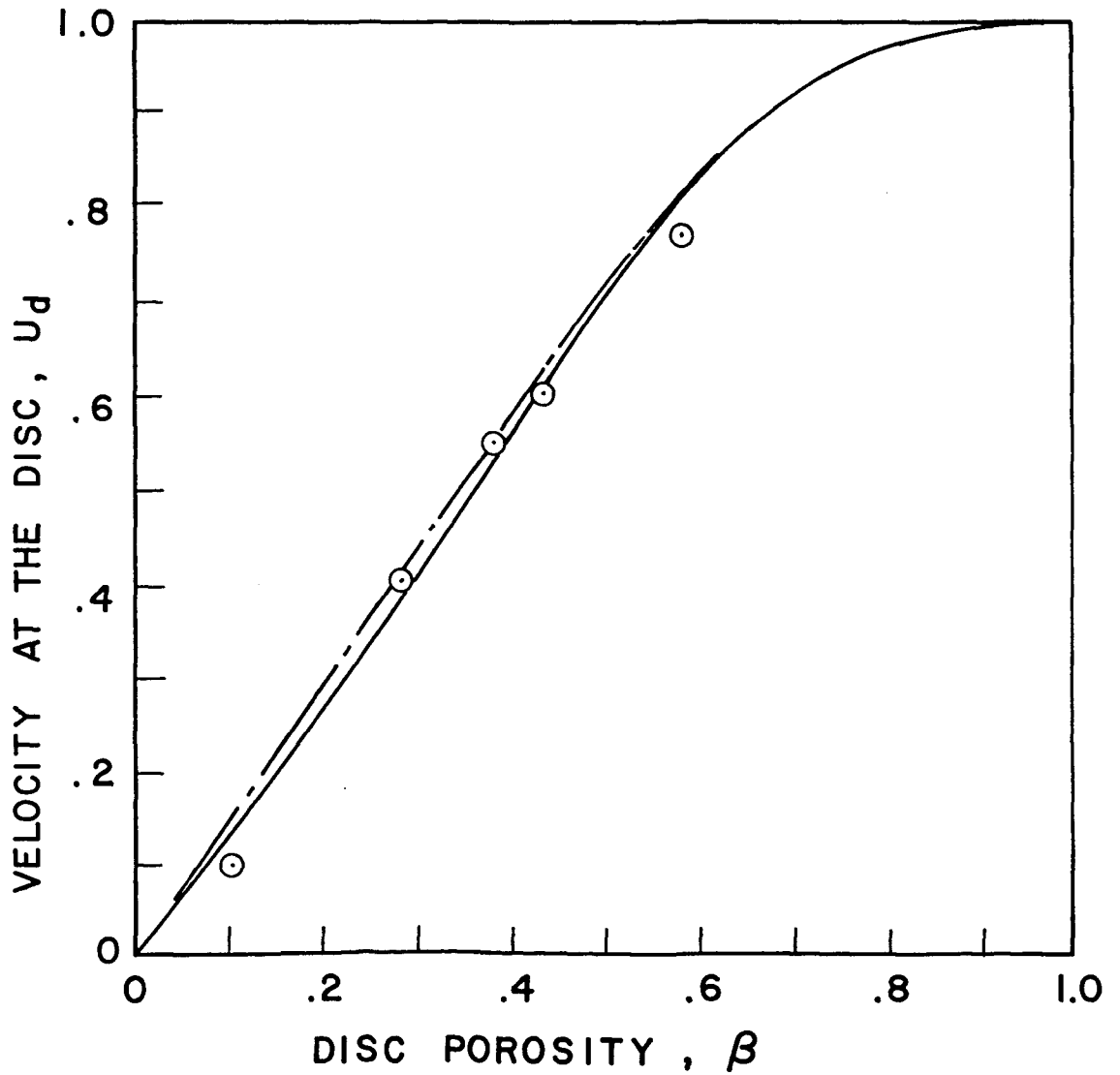
**FIGURE 6b – DRAG DISC REGION OF PERFORATED TUBE**



RELATION BETWEEN CROSS FLOW VELOCITY AND  
THE PRESSURE DIFFERENCE ACROSS THE WALL

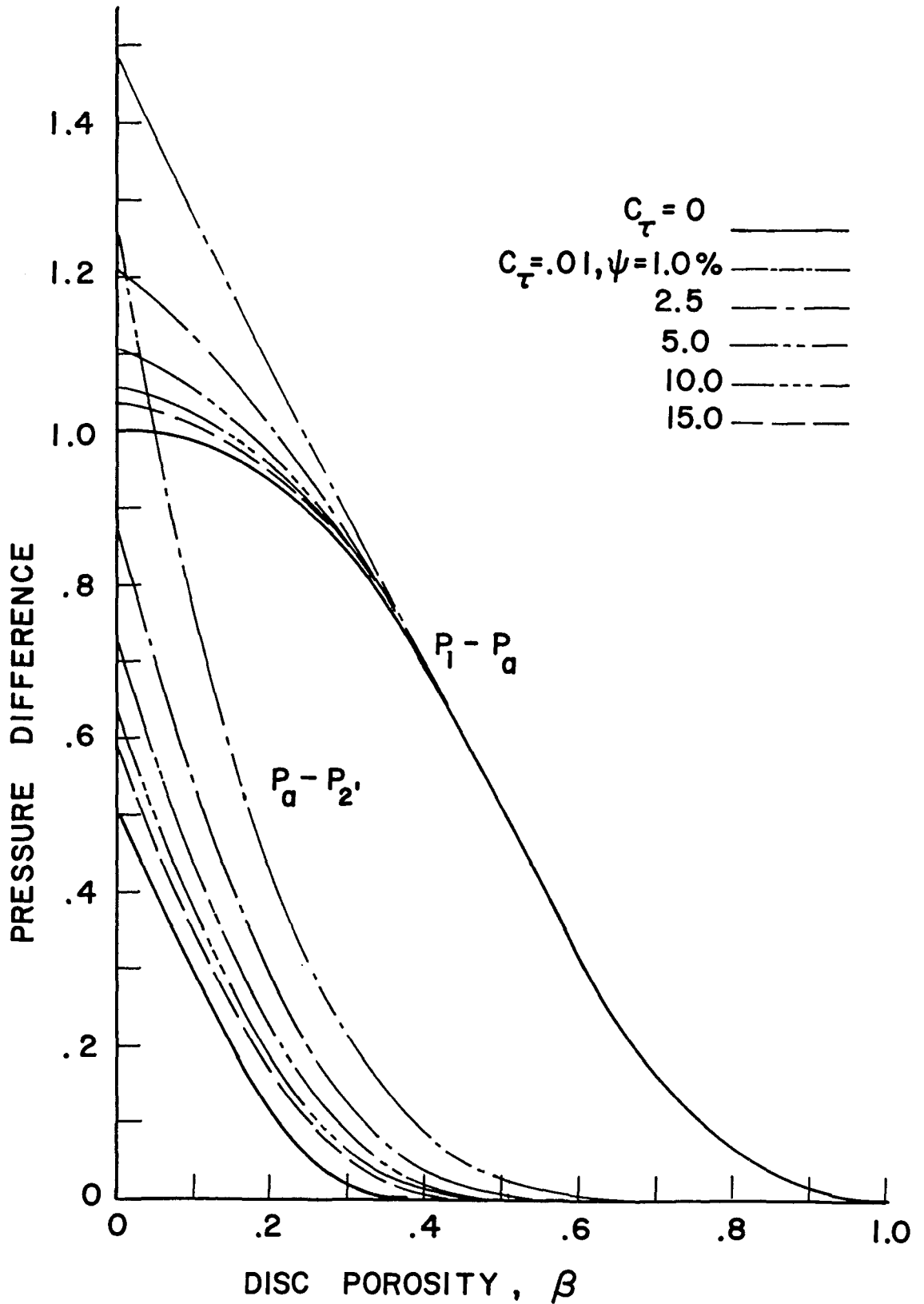
FIGURE 7

— INVISCID  
 - - - VISCOUS  $C_T = .01$   
 $\psi = 2.5\%$   
 ○ TAYLOR (REF. 11)



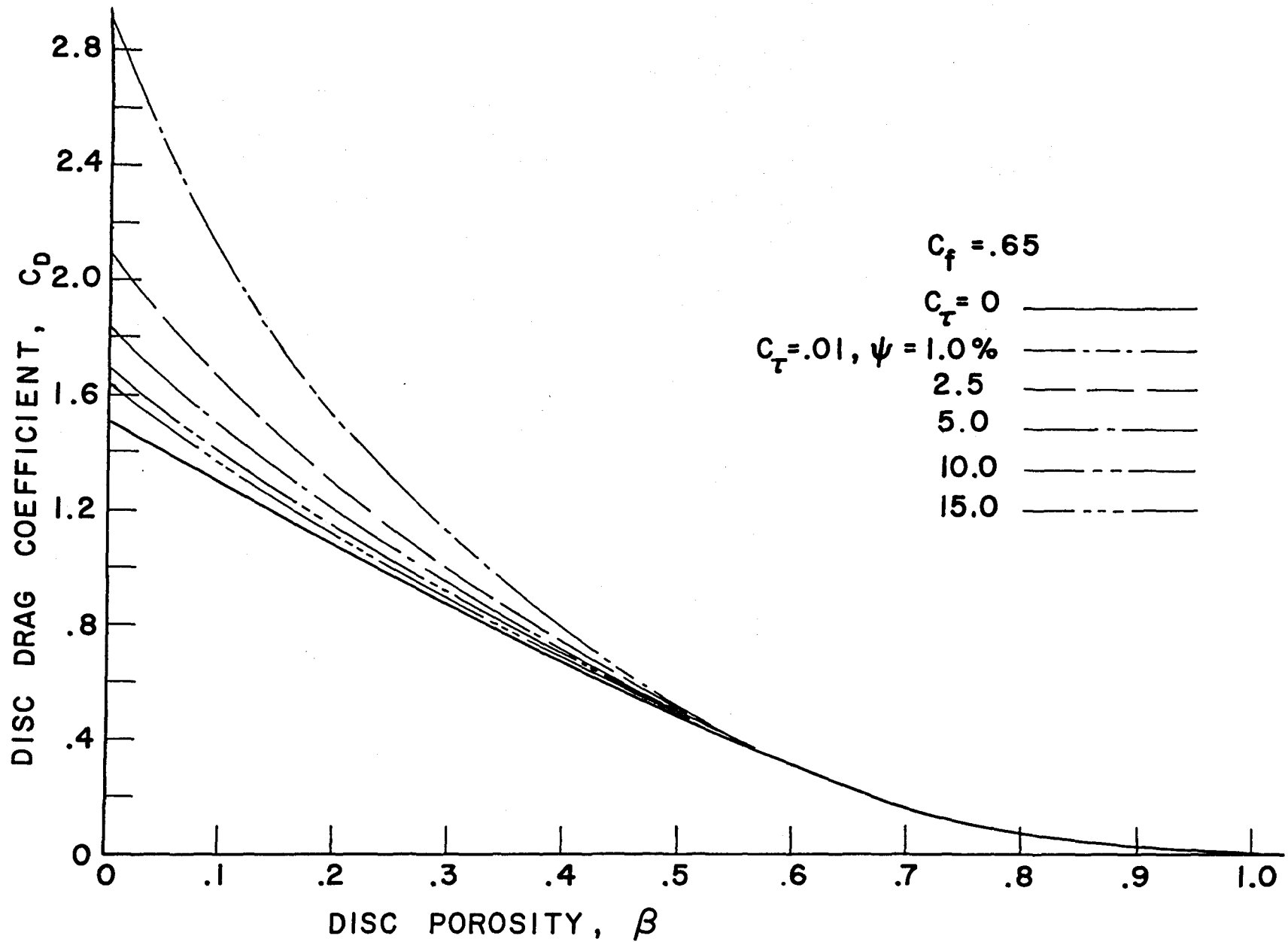
VELOCITY,  $U_d$  THROUGH THE DISC AS A  
FUNCTION OF THE DISC POROSITY

FIGURE 8

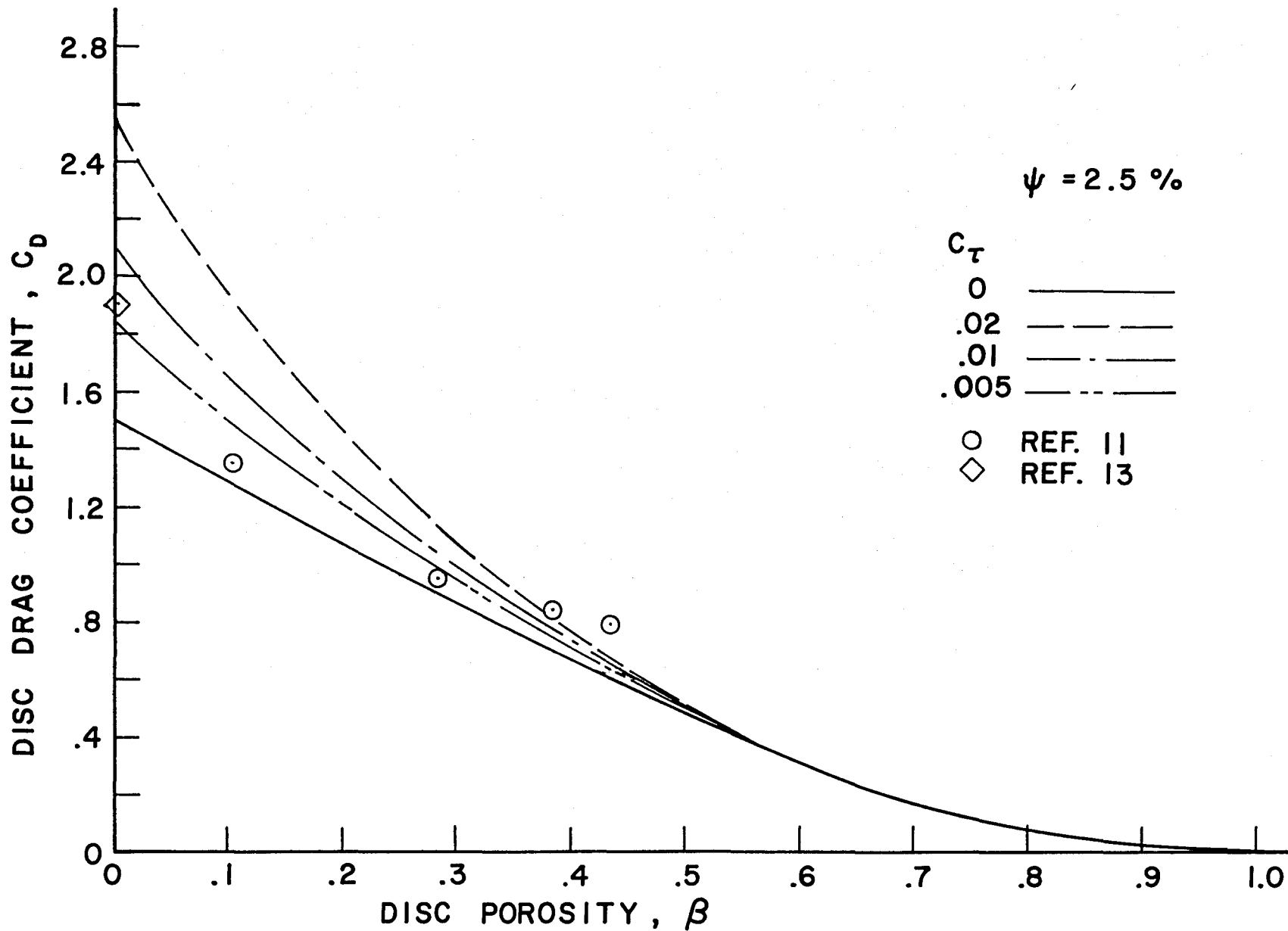


PRESSURE DIFFERENCE ACROSS THE WALL AT  
THE DRAG DISC VERSUS DISC POROSITY

FIGURE 9



DISC DRAG COEFFICIENT AS A FUNCTION OF DISC POROSITY  
 VARIOUS WALL POROSITIES — FIGURE 10



DISC DRAG COEFFICIENT AS A FUNCTION OF DISC POROSITY FOR VARIOUS TUBE WALL FRICTION FACTORS — FIGURE 11

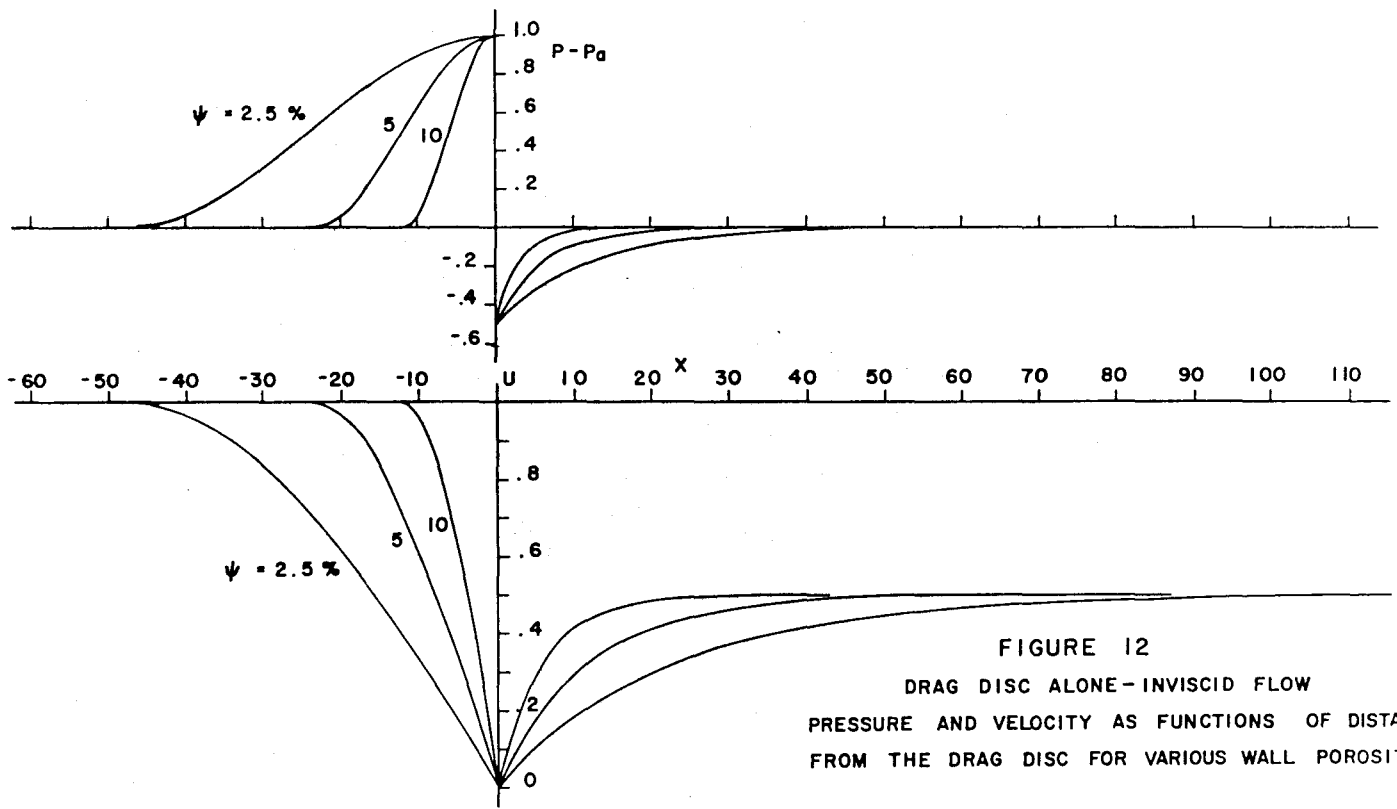


FIGURE 12  
 DRAG DISC ALONE-INVISCID FLOW  
 PRESSURE AND VELOCITY AS FUNCTIONS OF DISTANCE  
 FROM THE DRAG DISC FOR VARIOUS WALL POROSITIES

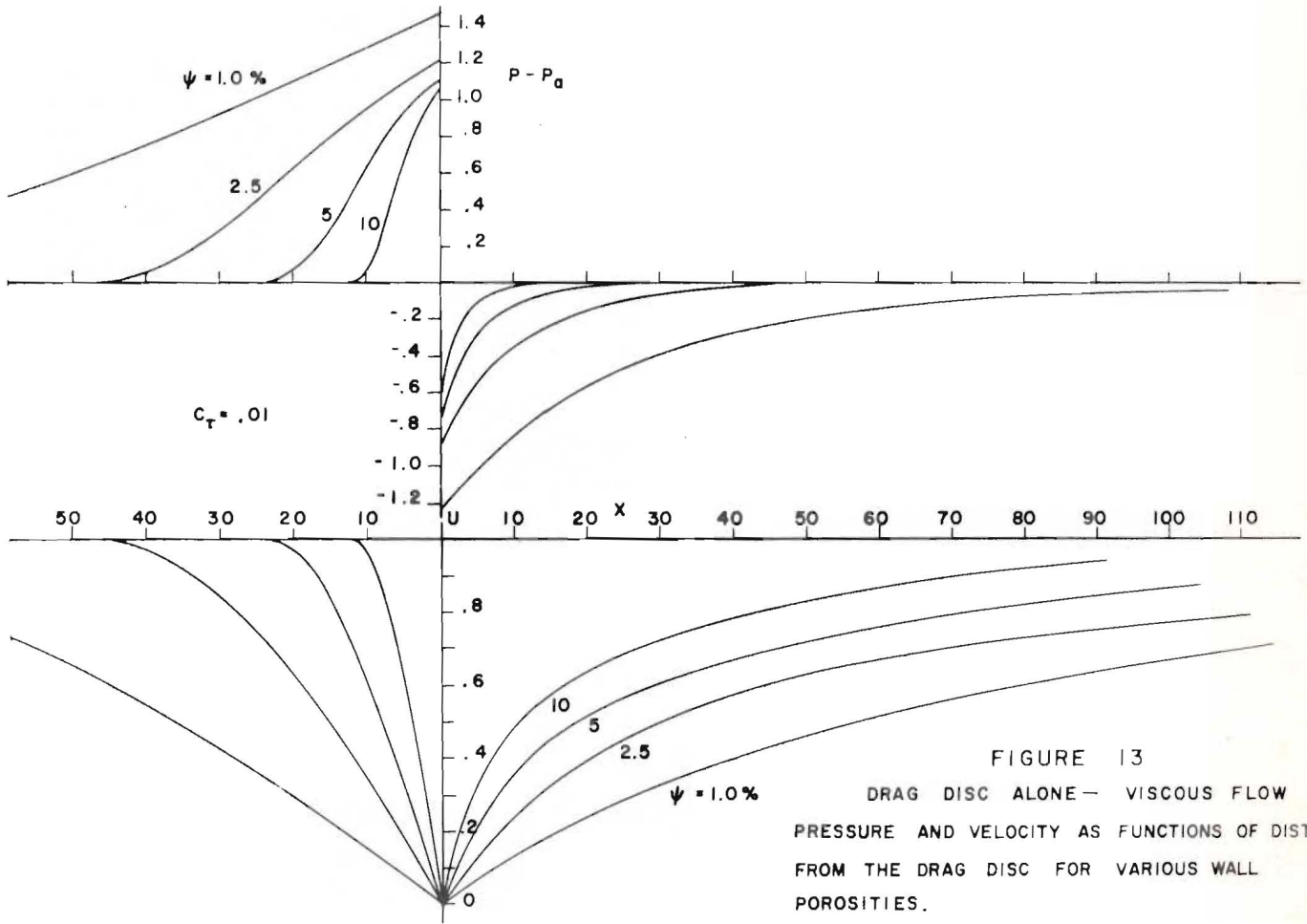
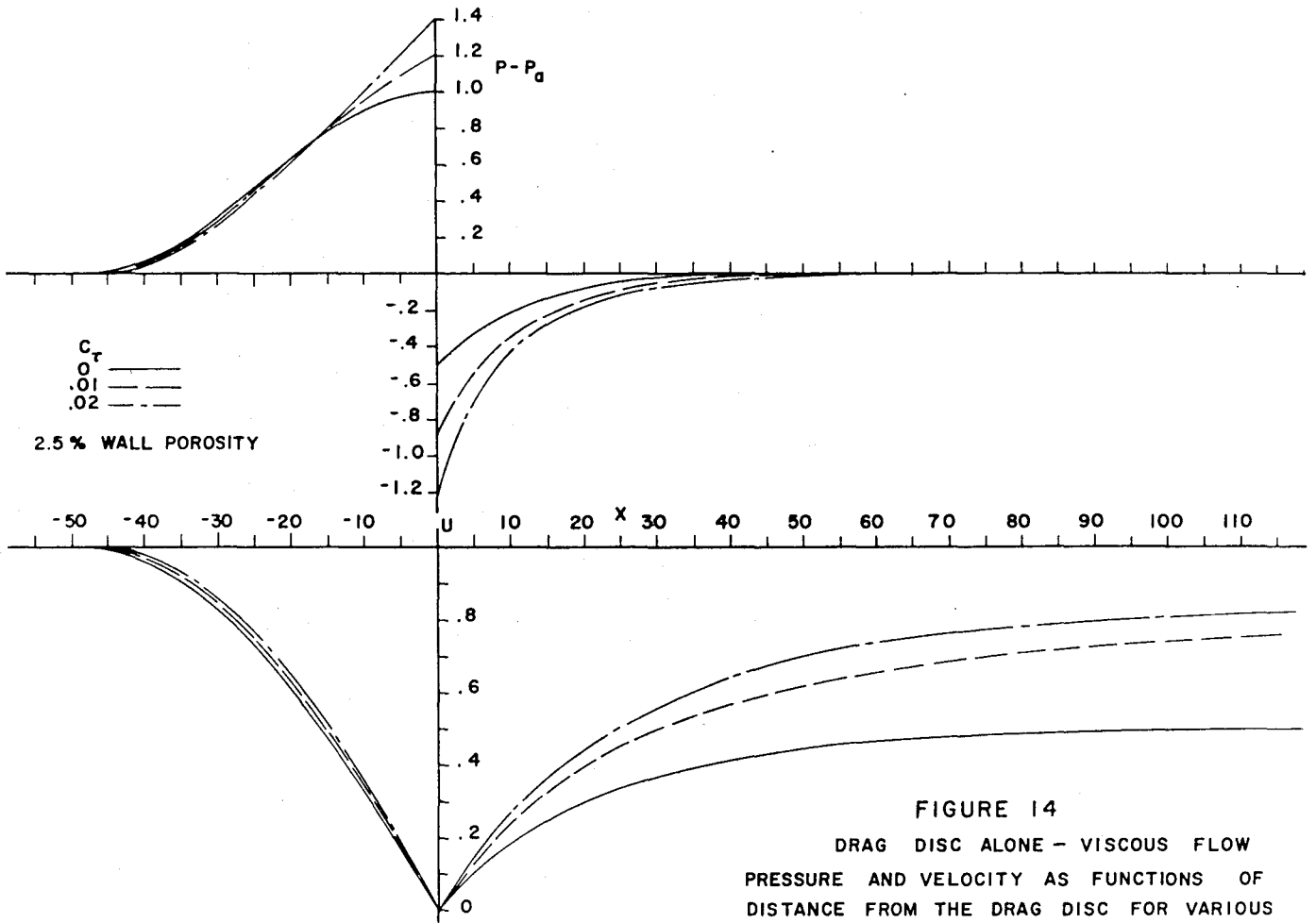
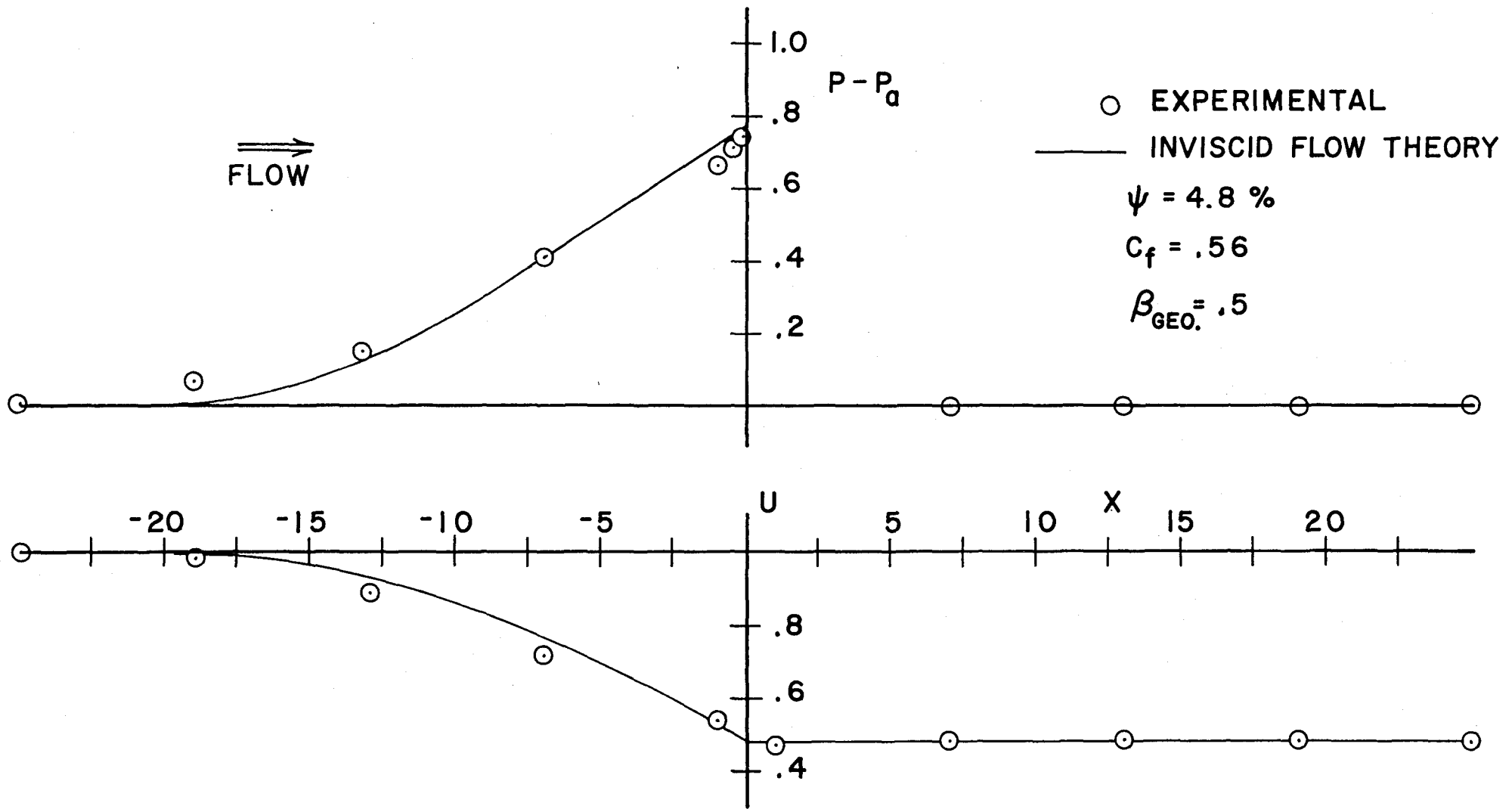


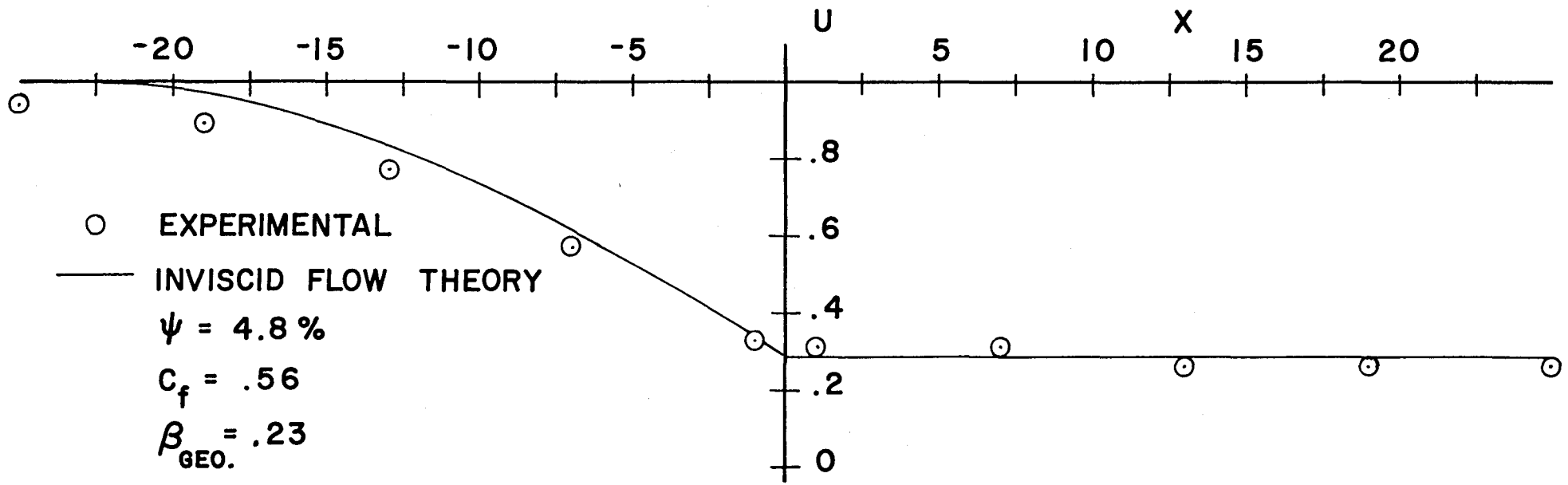
FIGURE 13  
 DRAG DISC ALONE— VISCIOUS FLOW  
 PRESSURE AND VELOCITY AS FUNCTIONS OF DISTANCE  
 FROM THE DRAG DISC FOR VARIOUS WALL  
 POROSITIES.





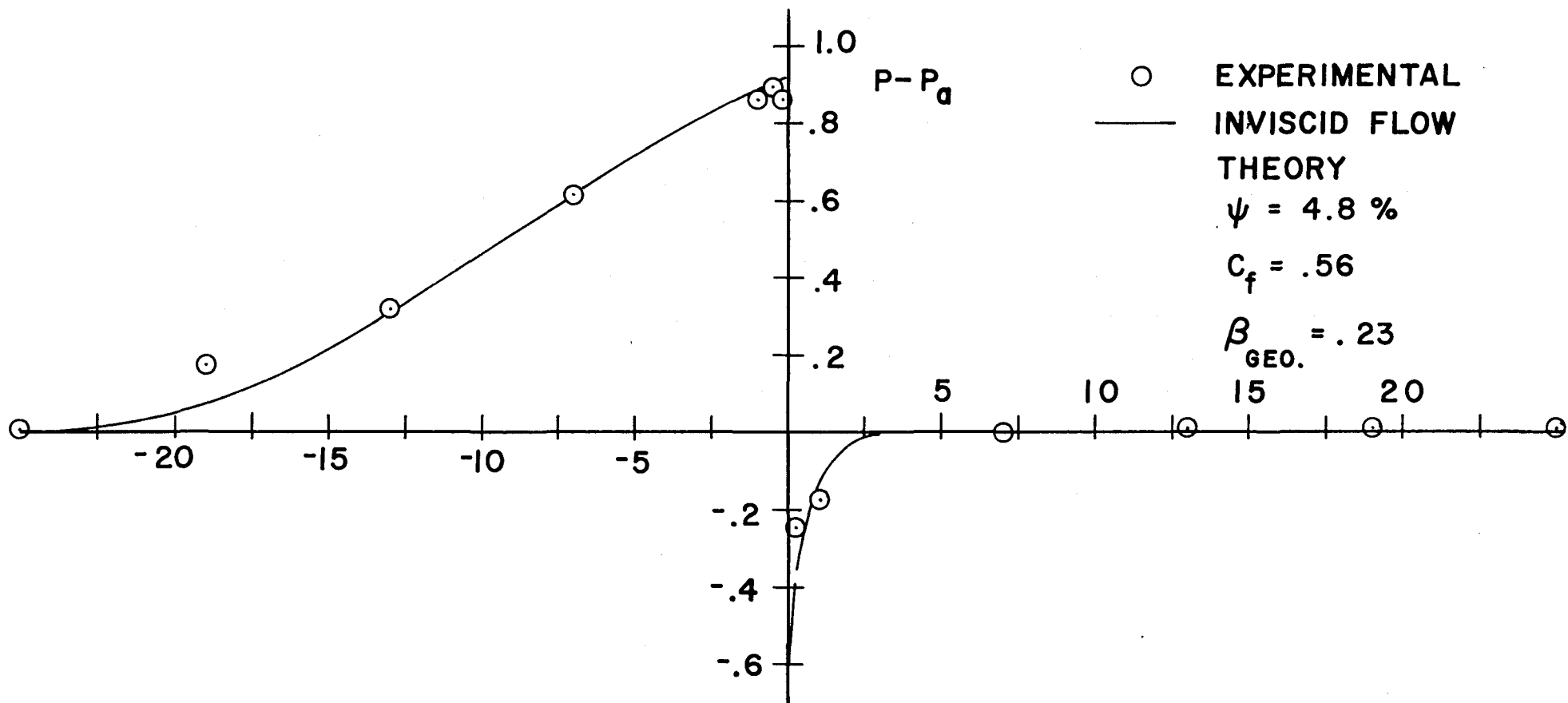
DRAG DISC ALONE      STATIONARY TUBE-WALL PRESSURE  
 AND VELOCITY AS FUNCTIONS OF DISTANCE FROM  
 THE DRAG DISC

FIGURE 15



DRAG DISC ALONE — STATIONARY WALL VELOCITY  
 AS A FUNCTION OF DISTANCE FROM THE  
 DRAG DISC

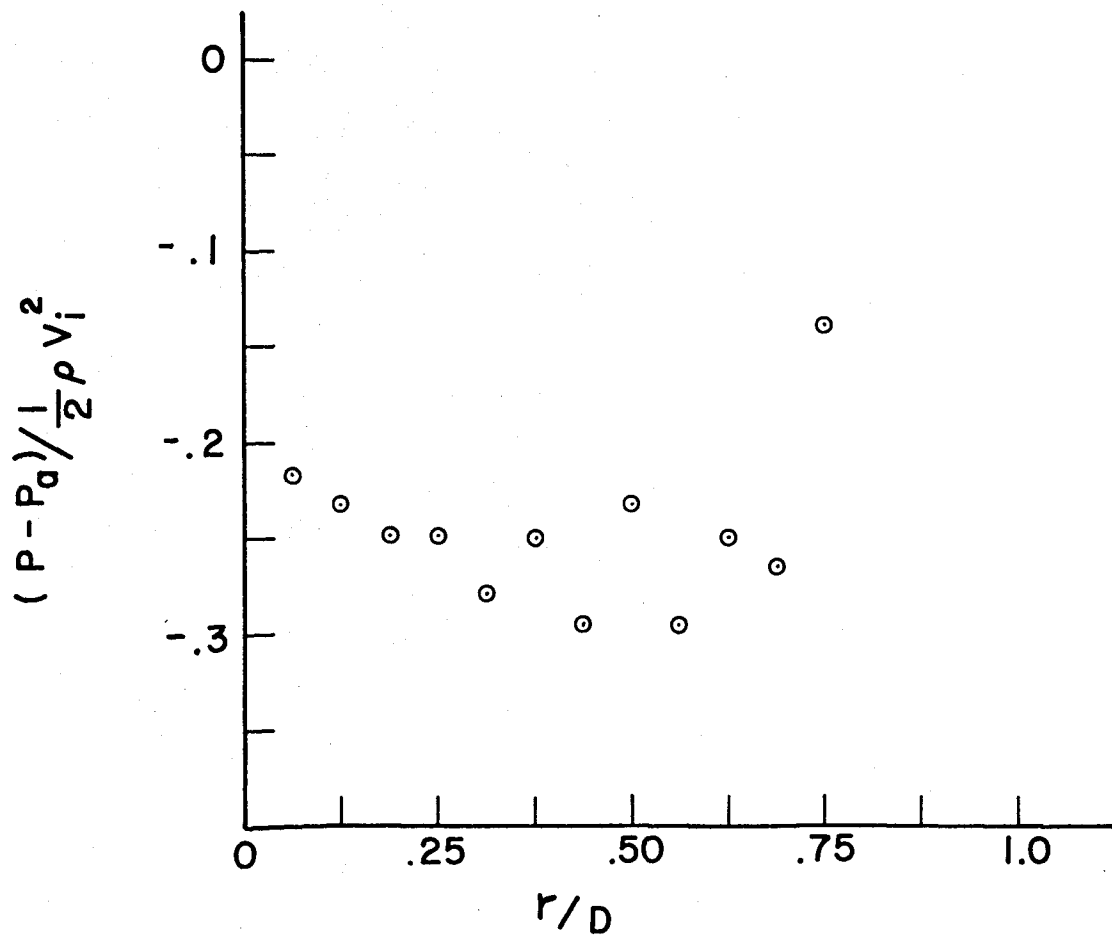
FIGURE 16a



DRAG DISC ALONE - STATIONARY WALL

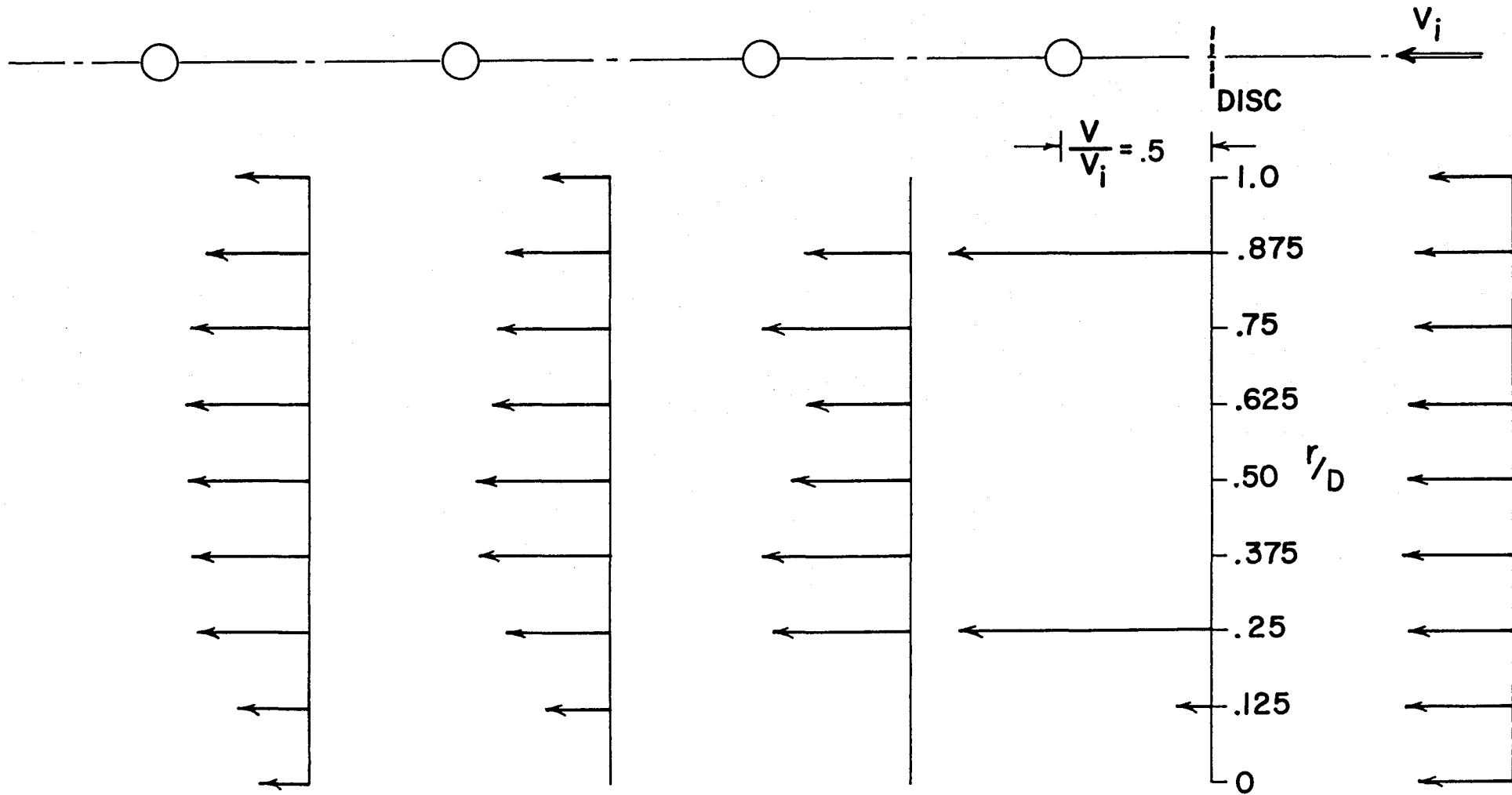
PRESSURE AS A FUNCTION OF DISTANCE FROM THE DRAG DISC

FIGURE 16b



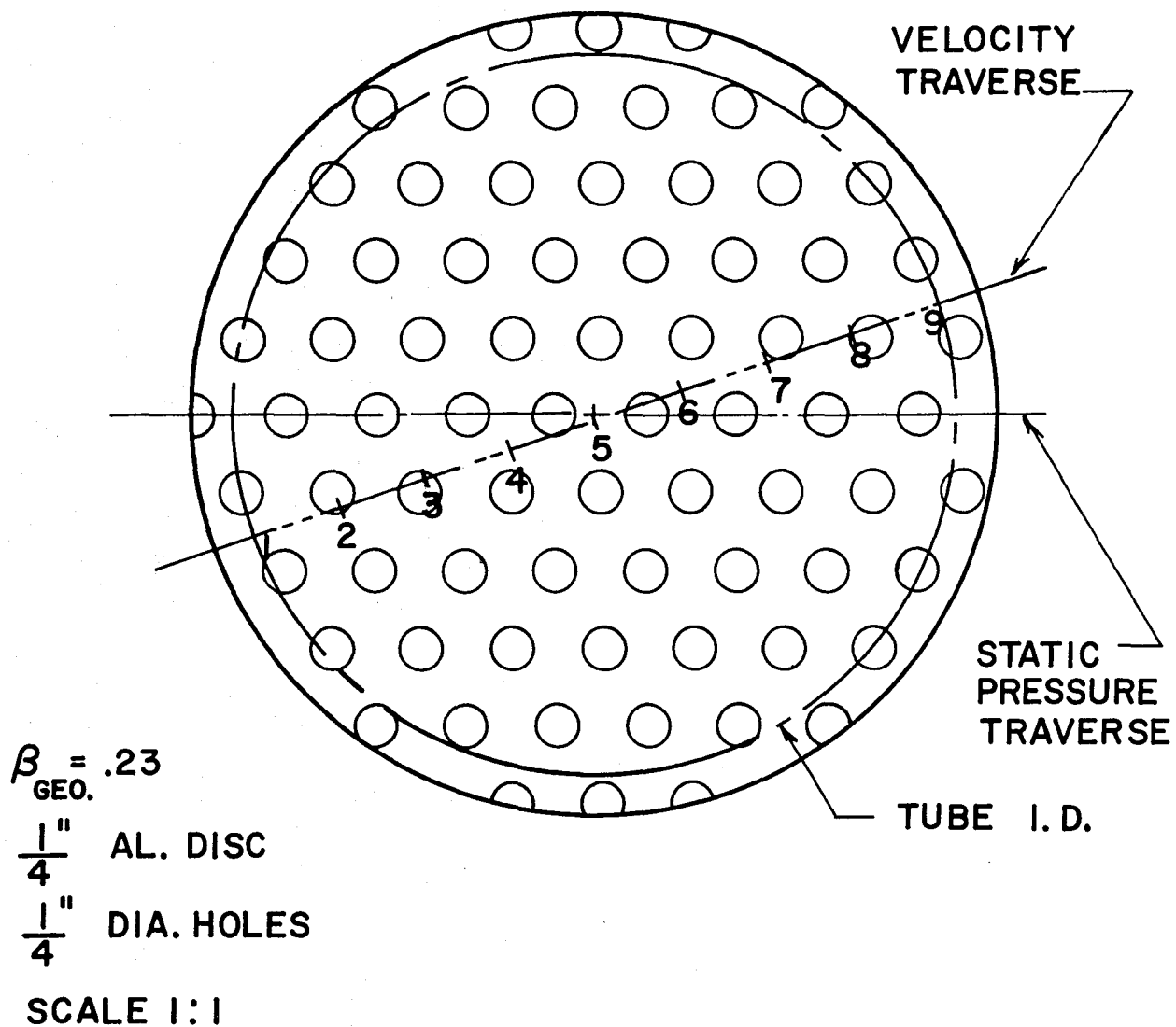
STATIC PRESSURE TRAVERSE IMMEDIATELY  
BEHIND THE DRAG DISC —  $\beta_{\text{GEO.}} = .23$

FIGURE 17



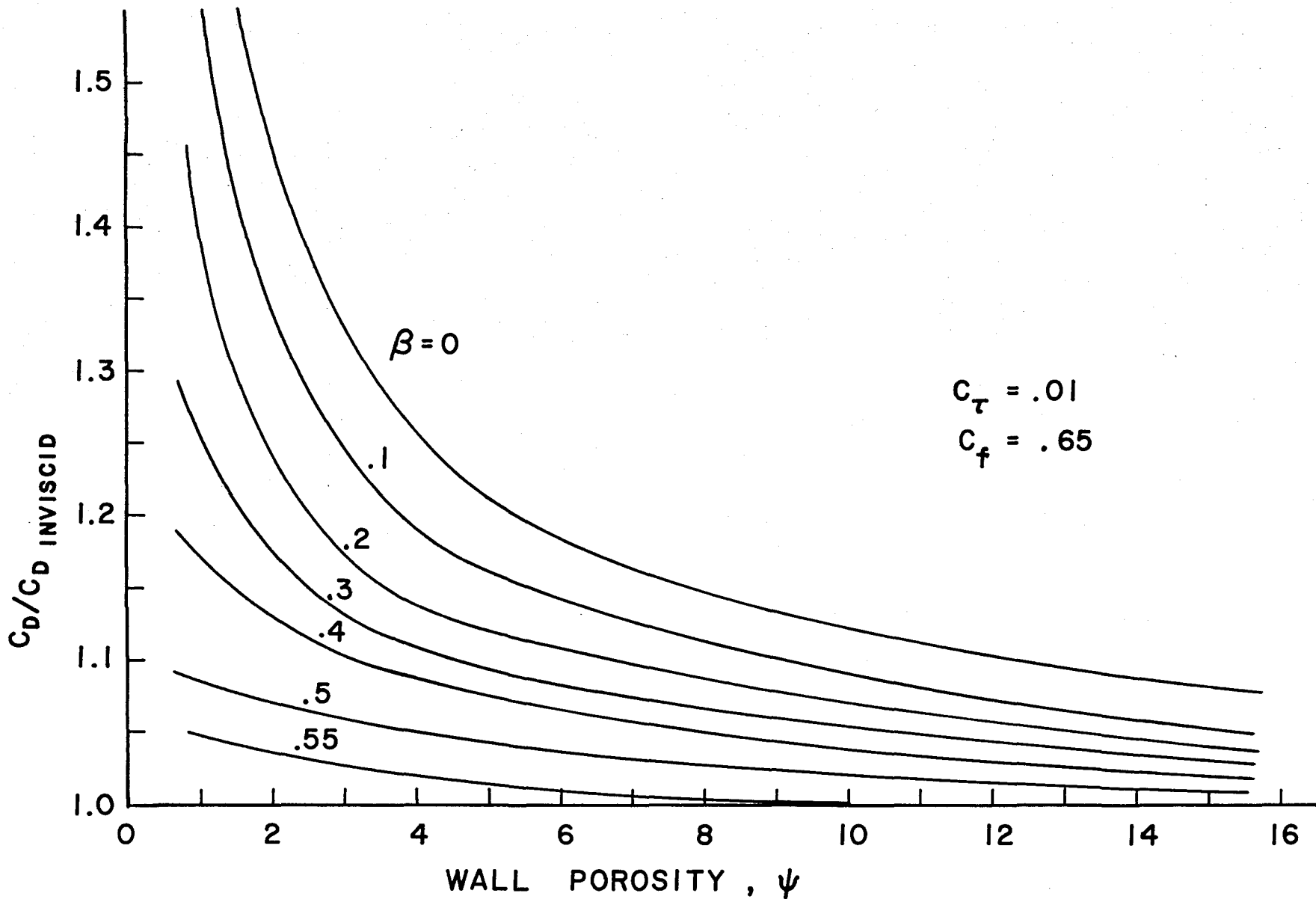
VELOCITY PROFILES IN THE NEIGHBORHOOD OF A DRAG DISC  
 IN A PERFORATED - WALL TUBE -  $\beta_{GEO.} = .23$

FIGURE 18

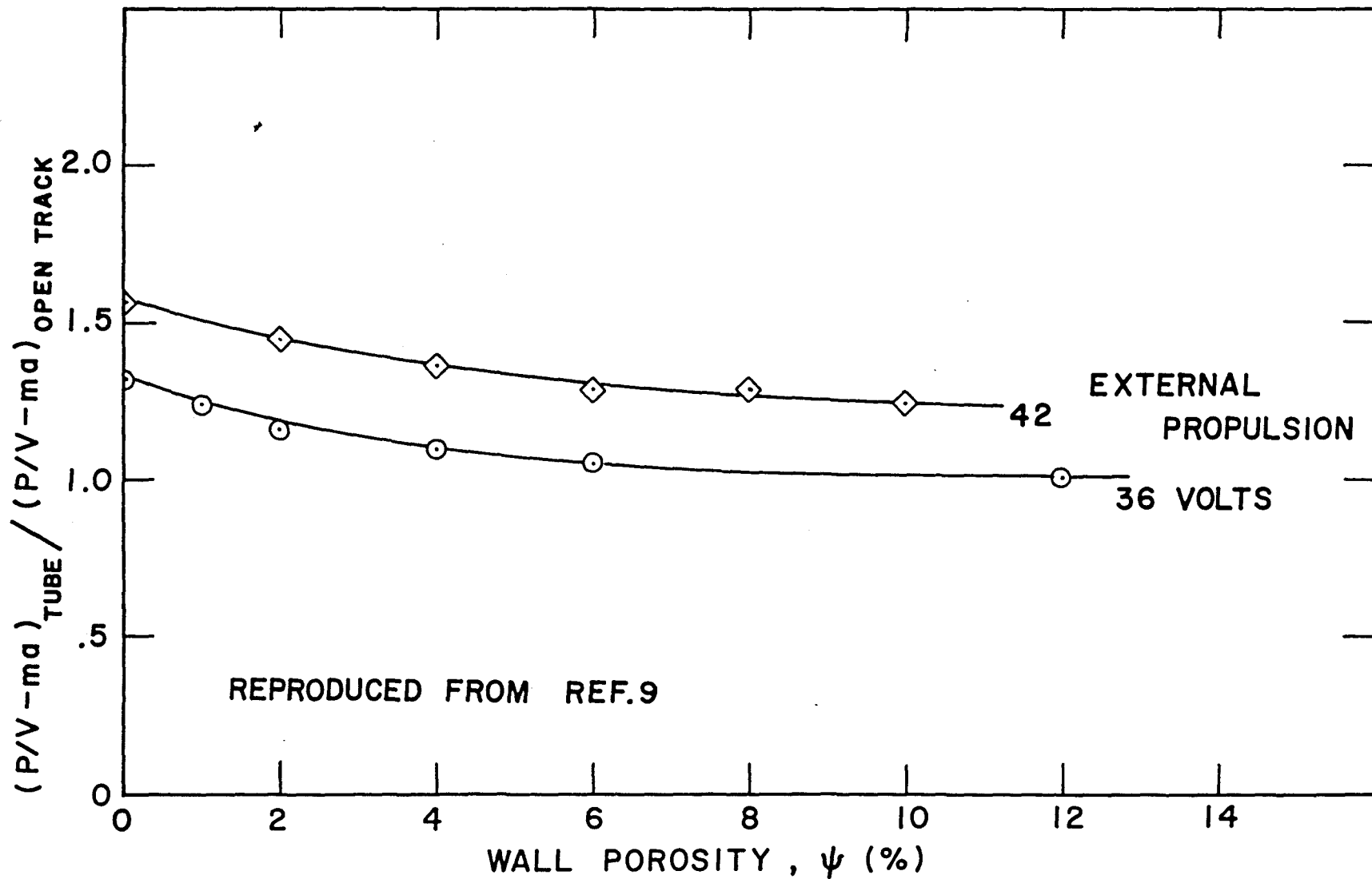


PERFORATED DISC SHOWING DIRECTION  
OF VELOCITY AND PRESSURE TRAVERSE

FIGURE 19



RATIO OF VISCOUS TO INVISCID DRAG COEFFICIENTS AS A  
 FUNCTION OF WALL POROSITY FOR VARIOUS DISC POROSITIES



REPRODUCED FROM REF.9

EFFECT OF TUBE WALL POPOSITIVITY ON THE EFFECTIVE DRAG RATIO AT VEHICLE TERMINAL SPEEDS — FIGURE 21

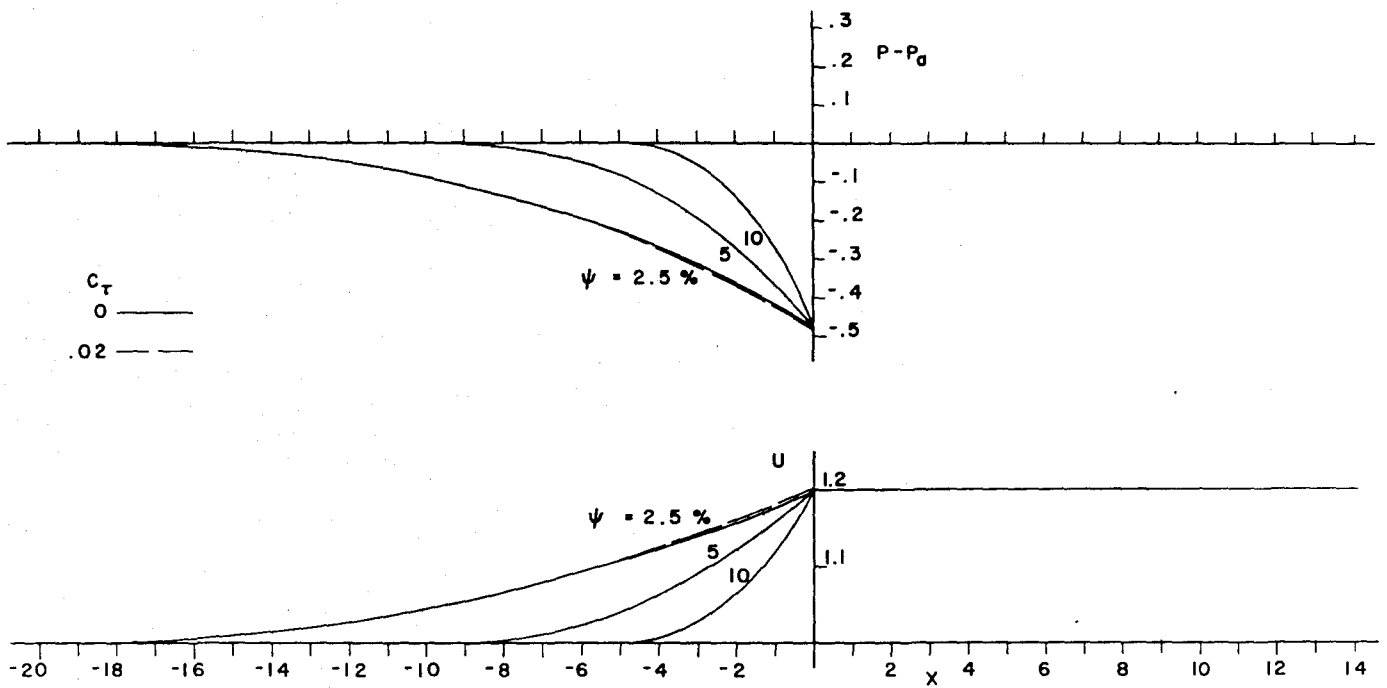


FIGURE 22  
 ACTUATOR DISC ALONE  
 PRESSURE AND VELOCITY AS FUNCTIONS OF  
 DISTANCE FROM THE ACTUATOR DISC FOR  
 VARIOUS WALL POROSITIES

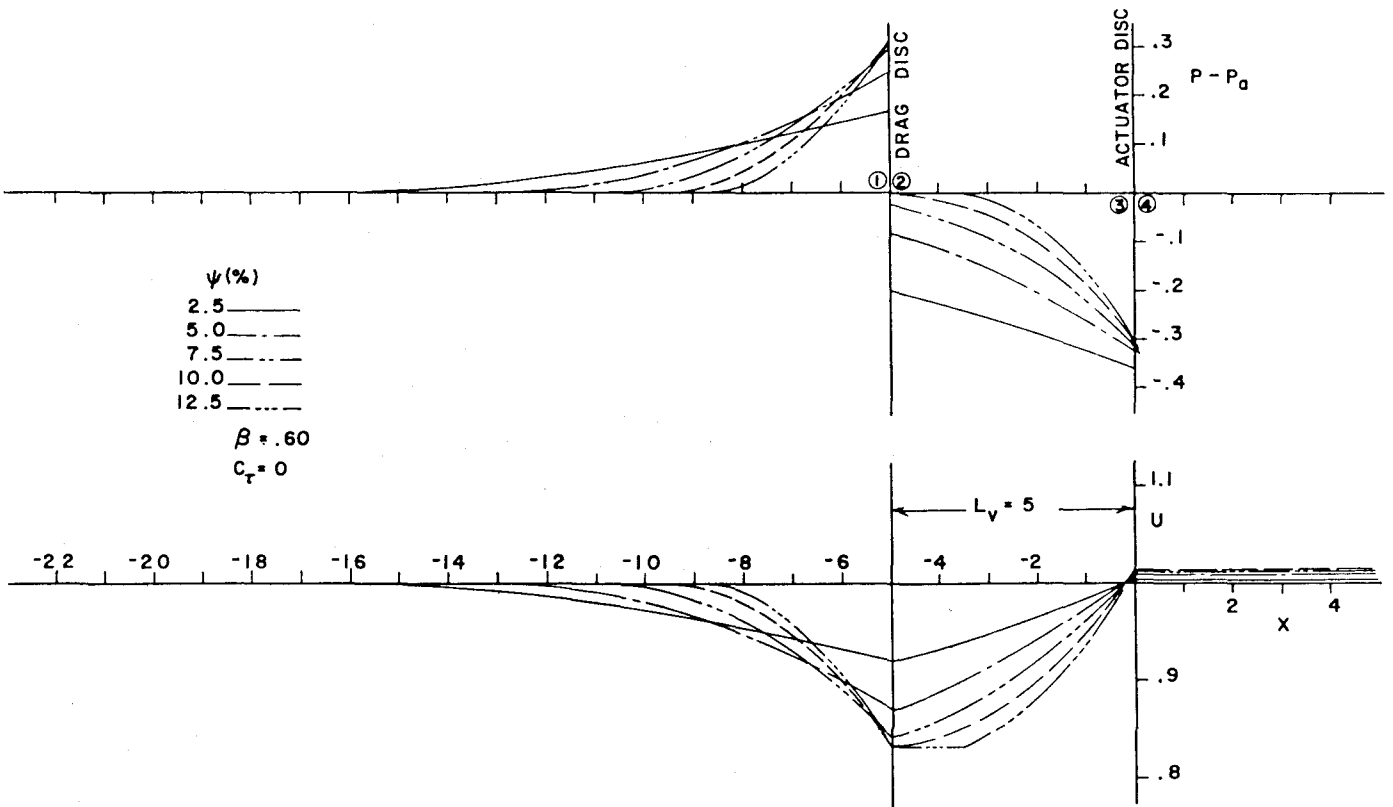


FIGURE 23  
 SIMULATED INTERNALLY PROPELLED VEHICLE  
 EFFECT OF VARIATION OF WALL POROSITY ON PRESSURE  
 AND VELOCITY DISTRIBUTIONS

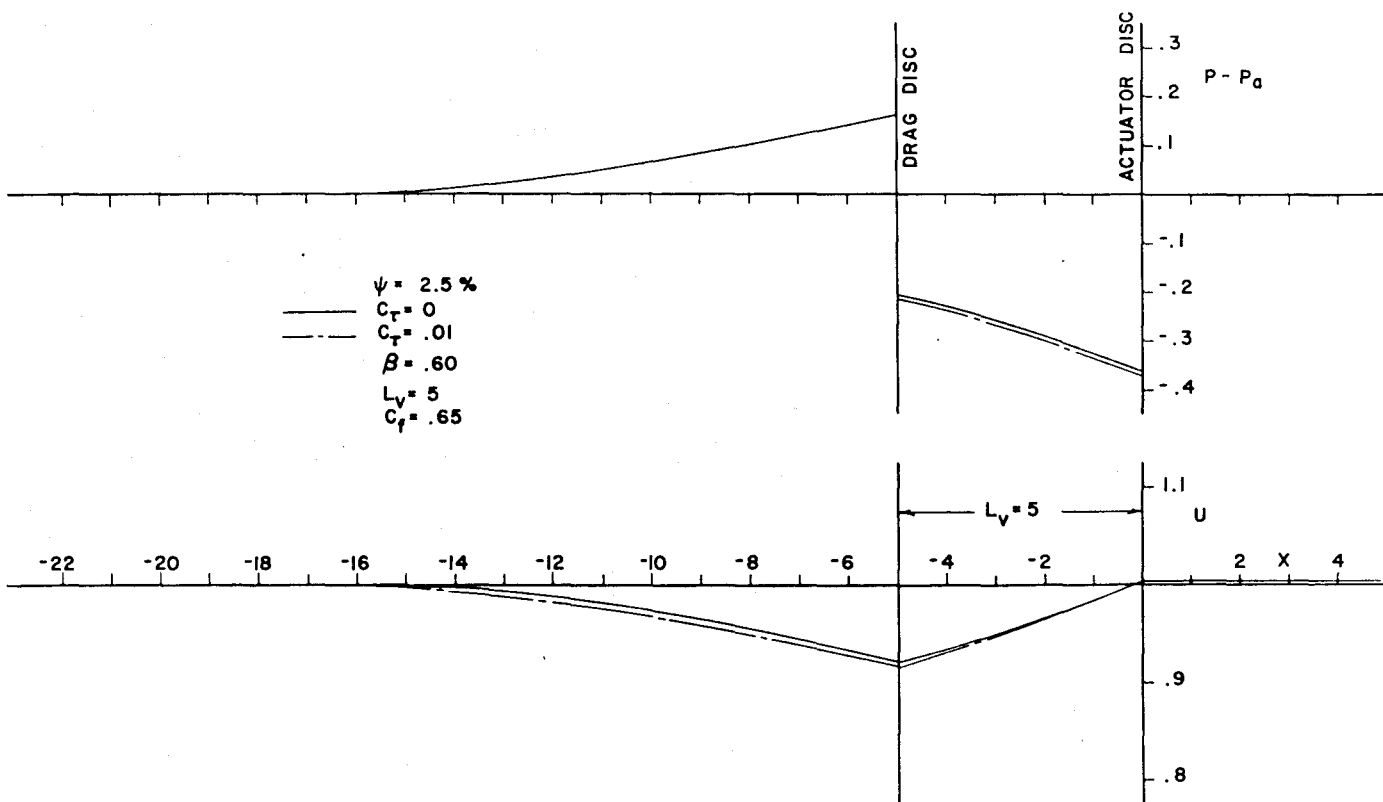


FIGURE 24  
 SIMULATED INTERNALLY PROPELLED VEHICLE  
 EFFECT OF VISCOSITY ON PRESSURE AND VELOCITY  
 DISTRIBUTIONS



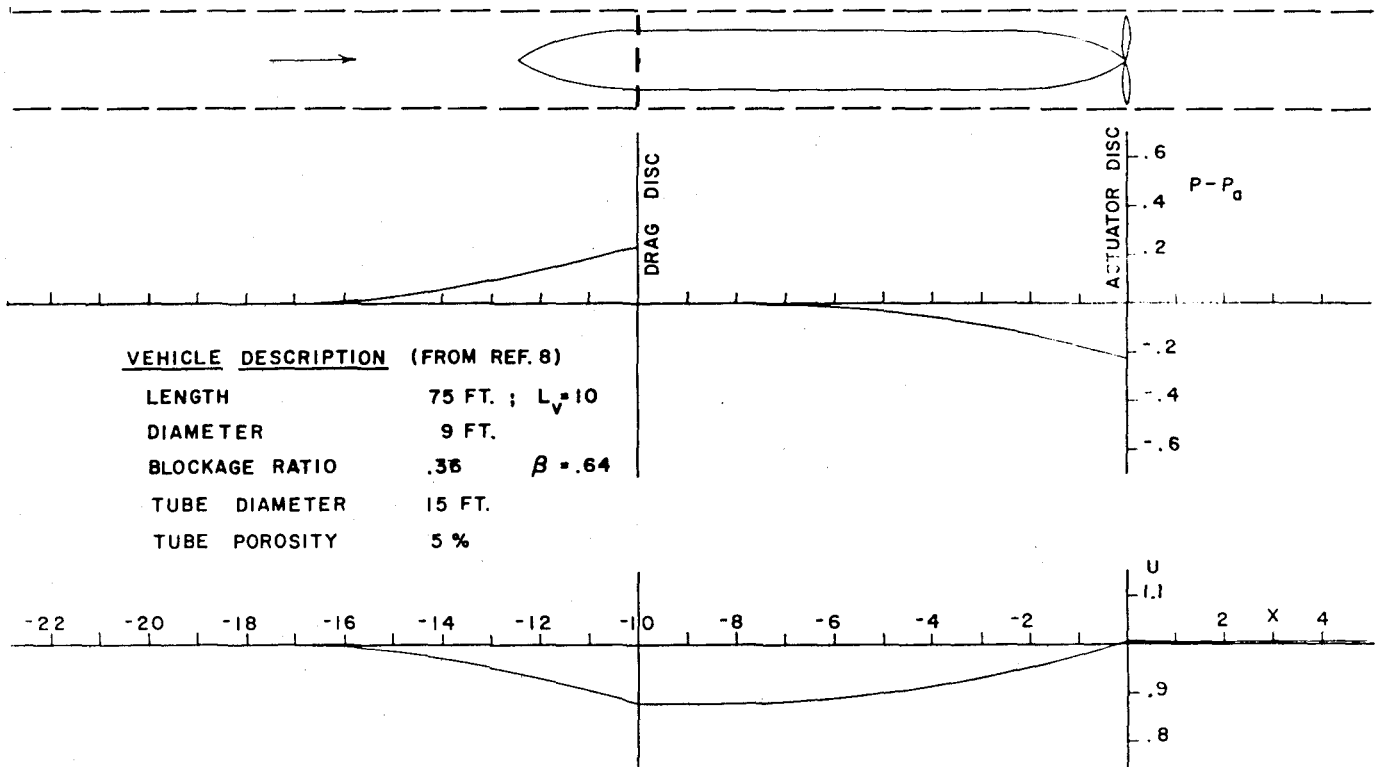


FIGURE 26  
SIMULATED INTERNALLY PROPELLED TUBEFLIGHT  
VEHICLE IN A 5 PER CENT POROUS TUBE

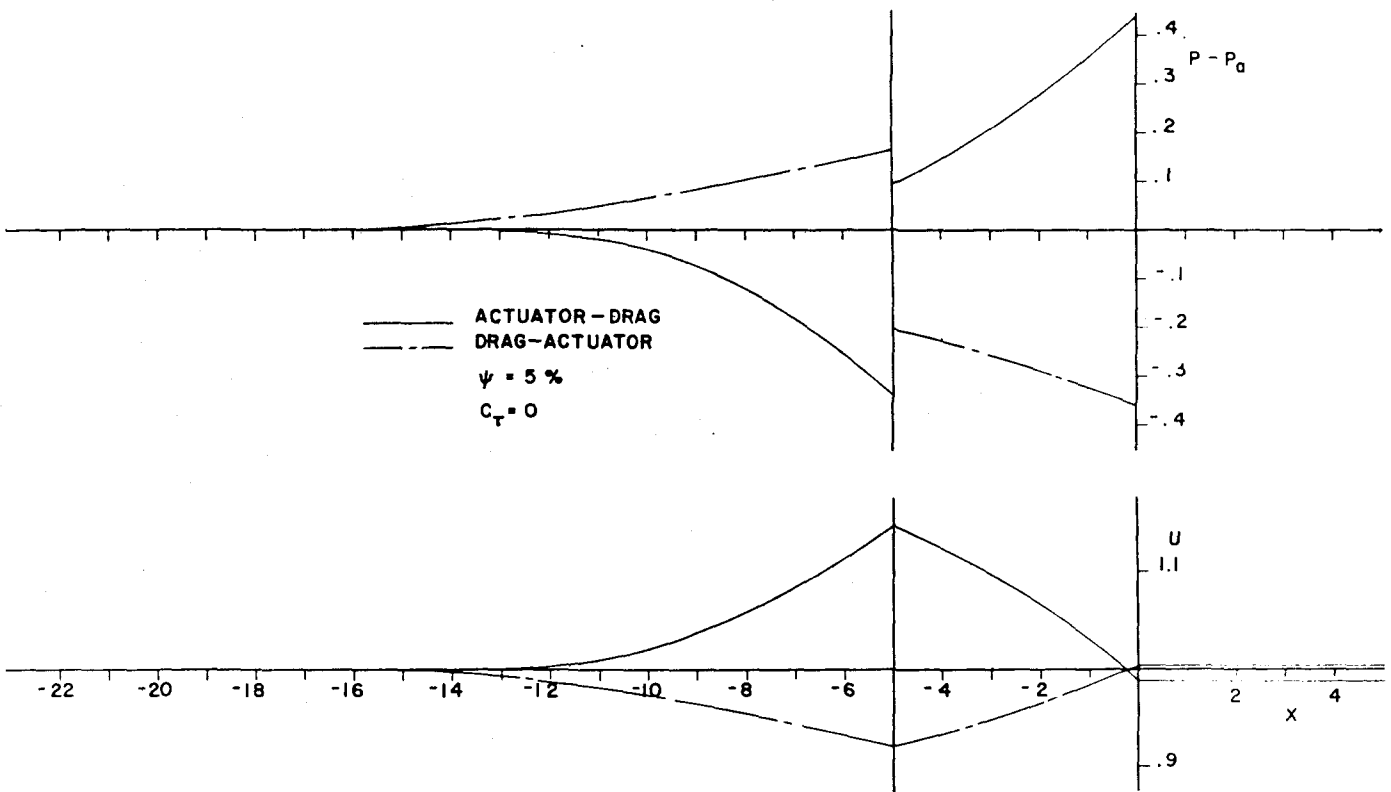
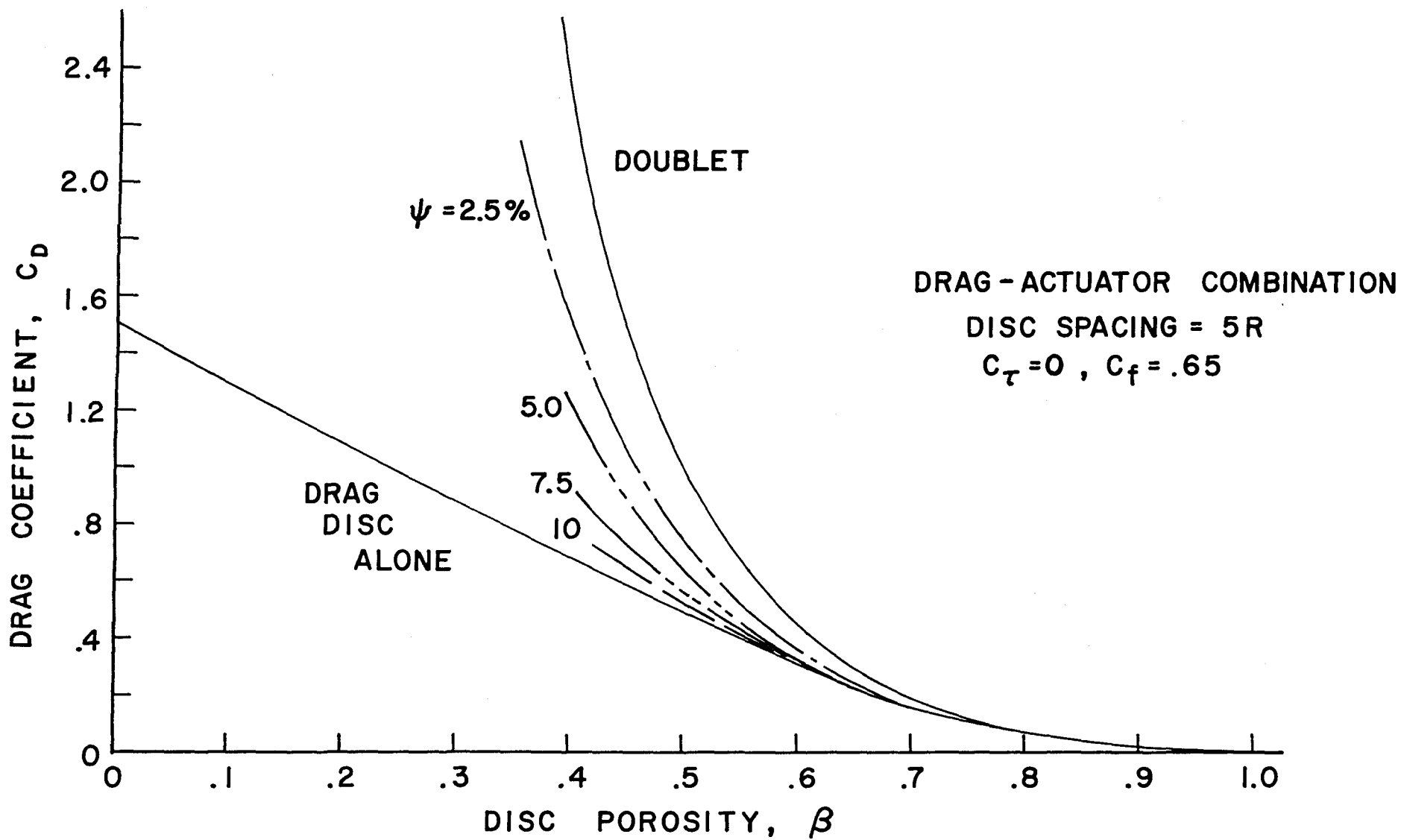
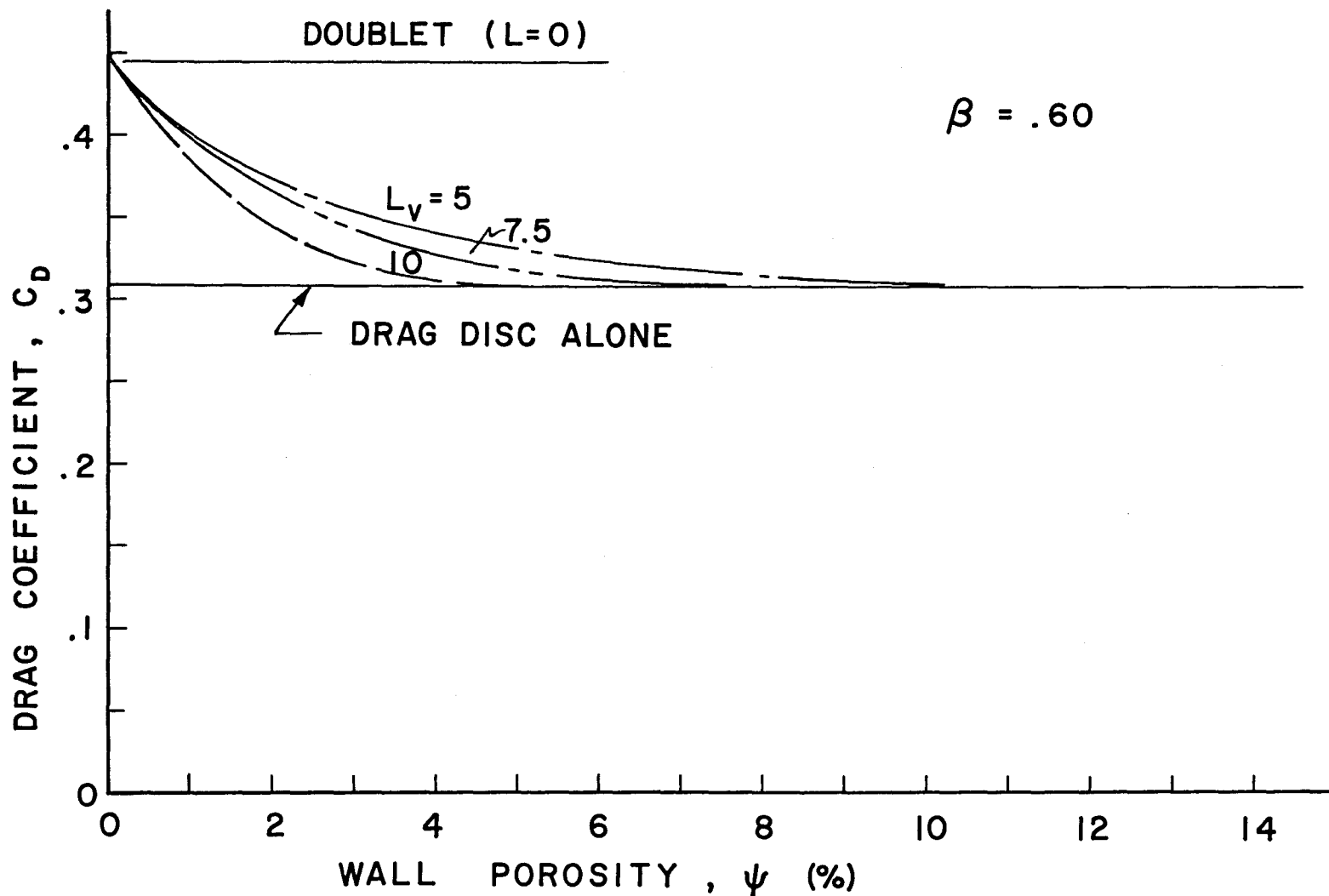


FIGURE 27  
 SIMULATED INTERNALLY PROPELLED VEHICLES  
 EFFECT OF FORE OR AFT POSITIONING OF THRUST GENERATOR



SIMULATED INTERNALLY PROPELLED VEHICLE  
 DRAG COEFFICIENT AS A FUNCTION OF DISC POROSITY FOR  
 VARIOUS WALL POROSITIES — FIGURE 28



SIMULATED INTERNALLY PROPELLED VEHICLE

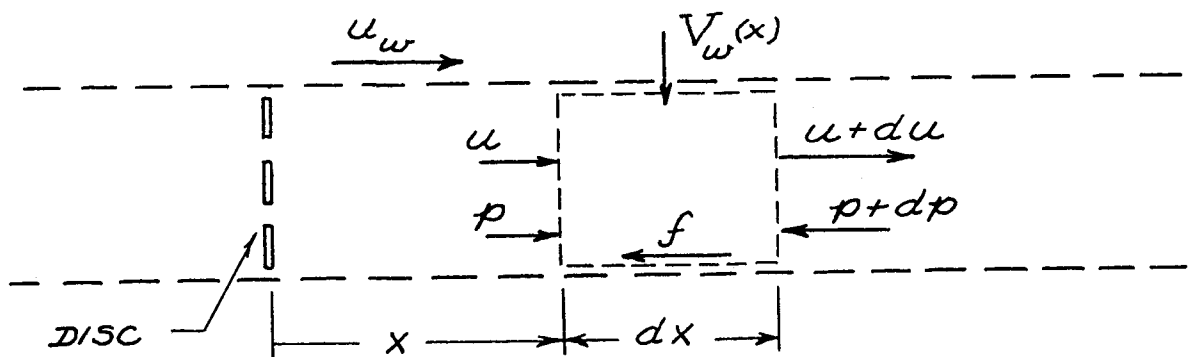
DRAG COEFFICIENT AS A FUNCTION OF WALL POROSITY

FIGURE 29

APPENDIX

DEVELOPMENT OF THE GOVERNING EQUATIONS

The control volume shown below is within an infinite, constant area, uniformly porous tube stationary in the vehicle or disc-fixed frame of reference. As such the walls and surrounding atmosphere are moving at a constant velocity  $u_w$  relative to the control volume.



The flow is steady in this frame of reference and is treated as one dimensional, incompressible and viscous with mass addition or extraction. Conservation of mass requires that

$$\rho \alpha (u + du) = \rho \alpha u + \rho A_h V_w(x) dx$$

or

$$du = \frac{A_h}{\alpha} V_w(x) dx$$

A-1

where  $A_h dx$  is the wall hole area over the tube length  $dx$ ,  $\alpha$  is the tube cross-sectional area and  $V_w(x)$  is the velocity through the wall at any given distance  $x$ .  $V_w(x)$  is positive or negative depending on whether for inflow or outflow. The flow through the wall is assumed to be proportional to the square root of the pressure difference across the wall. This means

that each hole is assumed to be a simple orifice. Thus  $V_w(x)$  may be expressed as

$$V_w(x) = C_{f1} \sqrt{\frac{2}{\rho} (p_a - p)} \quad (\text{inflow})$$

$$V_w(x) = -C_{f1} \sqrt{\frac{2}{\rho} (p - p_a)} \quad (\text{outflow})$$

where  $C_{f1}$  is a flow coefficient which is less than or equal to unity.

Considering the force due to pressure and the viscous effects due to the moving wall, the momentum equation may be written as

$$\begin{aligned} p\alpha - \alpha(p+dp) - \rho\alpha f dx &= \rho\alpha(u+du)(u+du) \\ &\quad - \rho\alpha u^2 - \rho A_h V_w(x) u_s dx \end{aligned}$$

The last term on the right hand side represents the x-directed momentum flux of the mass that passes through the wall.  $u_s$  is the axial velocity of this mass. For inflow,  $u_s = u_w$  since the wall and ambient outside air are moving at the velocity  $u_w$ . For outflow,  $u_s = u$ , the local axial velocity of the flow. If the wall and atmosphere are stationary relative to the disc, then for inflow  $u_s = 0$  and for outflow  $u_s = u$ . The situation of a stationary disc and wall is representative of a wind tunnel arrangement.

The previous equation reduces to

$$dp = -\rho(2u - u_s) du - \rho f dx \quad \text{A-2}$$

The friction force per unit mass  $f$ , is proportional to the square of the flow velocity relative to the wall. For moving walls,  $f$  is given by

$$f = -\frac{C_T}{r} (u_w - u) |u_w - u|$$

while for stationary walls  $f$  is

$$f = -\frac{C_T}{r} u^2$$

For convenience, the following non-dimensionalized terms are defined:

$$P \equiv p / \frac{1}{2} \rho u_\infty^2$$

$$U \equiv u / u_\infty$$

$$X \equiv x / r$$

$$\psi \equiv n d^2 / 4D$$

where  $u_\infty$  equals  $u_w$  for moving walls. In non-dimensional form, eqs.

A-1 and A-2 become

$$dU = 2\psi C_f \sqrt{P_a - P} dX \quad (\text{inflow})$$

A-3

$$dU = -2\psi C_f \sqrt{P - P_a} dX \quad (\text{outflow})$$

$$dP = -2(2U - U_s) dU + 2C_T(1-U) |1-U| dX \quad \text{A-4}$$

With eq. A-4 written in terms of influence coefficients as

$$dP = f_1 dU + f_2 dX$$

the various conditions are summarized in the table below.

|                  | $U_s$ | $f_1$      | $f_2$             |
|------------------|-------|------------|-------------------|
| <u>OUTFLOW</u>   |       |            |                   |
| Moving Walls     | $U$   | $-2U$      | $2C_T(1-U)/ 1-U $ |
| Stationary Walls | $U$   | $-2U$      | $-2C_T U^2$       |
| <u>INFLOW</u>    |       |            |                   |
| Moving Walls     | $1$   | $-2(2U-1)$ | $2C_T(1-U)/ 1-U $ |
| Stationary Walls | $0$   | $-4U$      | $-2C_T U^2$       |

Equations A-3 and A-4 can be combined to eliminate either X or P. Solving for dP/dU by the elimination of dX gives

$$\frac{dP}{dU} = -2U - \frac{2C_T}{\lambda} \frac{(1-U)|1-U|}{\sqrt{P-P_a}} \quad \text{A-5} \\ \text{OUTFLOW}$$

for outflow and

$$\frac{dP}{dU} = -2(2U-1) + \frac{2C_T}{\lambda} \frac{(1-U)|1-U|}{\sqrt{P_a-P}} \quad \text{A-6} \\ \text{INFLOW}$$

for inflow, where  $\lambda = 2\psi C_f$ .

The elimination of P and dP requires differentiating eqs. A-3 and equating to eq. A-4 to get

$$\frac{dU}{dX} \left( \frac{d^2U}{dX^2} + \lambda^2 U \right) - \lambda^2 C_T (1-U)|1-U| = 0 \quad \text{A-7} \\ \text{OUTFLOW}$$

for outflow and

$$\frac{dU}{dX} \left( \frac{d^2U}{dX^2} - \lambda^2 (2U-1) \right) + \lambda^2 C_T (1-U)|1-U| = 0 \quad \text{A-8} \\ \text{INFLOW}$$

for inflow.